

Recent Progress on Conductive Metal-Organic Framework Films

Xueyang Mu^a, Weike Wang^{a,}, Chongcai Sun^a, Jiulong Wang^a, Chengbing Wang^{a,*}, and Mato Knez^{b,c,*}*

X. Y. Mu, Dr. W. K. Wang, C. C. Sun, J. L. Wang, Prof. C. B. Wang

School of Materials Science and Engineering

Shaanxi Key Laboratory of Green Preparation and Functionalization for Inorganic Material

Shaanxi University of Science & Technology

Xi'an, Shaanxi 710021, P. R. China.

E-mail:wangweike@sust.edu.cn; wangchengbing@gmail.com

Prof. M. Knez

CIC nanoGUNE

Tolosa Hiribidea, 76, E-20018, Donostia-San Sebastian, Spain

Prof. M. Knez

IKERBASQUE

Basque Foundation for Science

E-48013, Bilbao, Spain

E-mail:m.knez@nanogune.eu

Keywords: preparation of MOF films, introduction of conductivity, doping, conductive MOFs films, applications

Because of their outstanding structural, chemical, and functional diversity, Metal-organic frameworks (MOFs) have brought about worldwide interest over the last two decades, which have been utilized in a wide range of applications in the fields of gas separation, storage, catalysis and drug delivery. However, among these applications, MOFs are almost used in the form of powder. Due to their fragility and difficulty in preparing large-area thin film materials, the study of MOF films and their electronic properties is a challenging problem in the research of MOFs . Owing to the low-energy charge transport mode, most MOF films are essentially insulating, which largely limits their applications in fields where electronic charge transport takes place, such as electronics or electrochemistry. So, the introduction of

conductivity into the MOF films opened the new avenues for their applications in electrochemical sensing, supercapacitors, batteries, electrocatalysis, and electronic devices and made the research on and with MOF films very active. Herein, we review the latest progress of conductive MOF films, including the preparation of MOF films, the design and adjustment strategies for constructing intrinsic and doping conductive MOF films, and their applications. In addition, the numerous challenges of conductive MOF films are also elaborated.

1. Introduction

Metal organic frameworks (MOFs),^[1] known as porous coordination polymers,^[2] are a new kind of crystalline materials with periodic network structures prepared by the self-assembly of various metal ions and organic ligands via the formation of coordination bonds. About 1 million MOFs, with their related theoretical descriptions, have been obtained by changing the types of metal ions and organic ligands. Because of their unique structure, MOFs have a number of advantages, including a large specific surface area, high crystallinity, good chemical stability and adjustable pore size, which are widely used in gas storage,^[3,4] separation,^[5,6] catalysis,^[7,8] drug delivery^[9] and other fields. Among most of aforementioned applications, MOFs are used in the form of powder. The study of thin film MOF materials and their electronic properties is a challenging problem in MOF research. Due to their low energy charge transfer pathways, most MOFs are insulators (having conductivities less than 10^{-10} S cm^{-1}).^[10] Thus, even though they have large specific surface areas and highly controllable porosity, it is difficult to apply MOFs in electronics and electrochemistry. Therefore, it is necessary to design and prepare MOF films with high conductivity and persistent porosity. The potential of MOFs as active materials in semiconductor research is recently being recognized. Conductive MOFs can be designed and regulated by (1) changing the metal ions,

(2) using typical organic ligands to directly synthesize conductive MOFs, or (3) post-synthetic modification of the MOFs by introducing guest molecules, or via other processes. For example, Park et al. shortened the S•••S distance between adjacent tetrathiofulvalene (TTF) nuclei in tetraphenyl conjugate (TTFTB)-based MOFs by increasing the cation size,^[11] from Zn²⁺ to Co²⁺, Mn²⁺, and Cd²⁺, which increased the overlap between the S 3pz orbitals, thus regulating electronic conductivity of the MOF. Marinescu *et al.* used THT, a redox active ligand, combined with various metal ions and the resulting FeTHT MOF film exhibited higher electronic conductivity after cooling and had metallic properties.^[12] Han et al. doped CO₃(NDC)₃ MOF thin films with I₂,^[13] changing a MOF that initially had insulating properties into a p-type semiconductor, due to charge-transfer-induced hole doping. All of these methods provide either "through space" or "through bond" charge transfer pathways in the materials,^[14,15] thereby promoting electron transport and improving the conductivity of the MOF. The "through bond" conduction in MOF depends on charge transport in the continuous valence band, in which charge transfer is promoted through covalent bond overlap between metal nodes and organic ligands with appropriate orbital symmetries and energies. In contrast, the "through space" method provides space and orbital overlap for charge transport via noncovalent interactions between electroactive segments of the metal-ligand bonds in the MOF, thus creating an extended charge transfer pathway.

In recent years, conductive MOF films have gained prominence as emerging electronic materials. These films overcome the limitations of MOF powders, which are fragile and difficult to prepare as large-area membrane materials. Moreover, conductive MOF thin films show significant capacity for application in energy storage, catalysis and sensing attributed to their high degree of orientation, high crystallinity, and controllable thickness. In 2015, Dincă *et al.* first applied conductive MOF to manufacture a chemical resistance sensor,^[16] exploiting the higher sensitivity of conductive MOF by using Cu₃(HITP)₂ rather than carbon nanotubes

(CNT) for sensing. In 2017, the Dincă group prepared $\text{Ni}_3(\text{HITP})_2$ as an electrode material for the electrochemical capacitors (EC),^[17] and found that this material has excellent capacitance. This major discovery has inspired scientists to explore applications of the conductive MOFs in the field of electrochemistry, including chemical resistance sensors,^[18-20] supercapacitors,^[21-24] electrocatalysis,^[25-27] and electronic devices.^[28-30]

At present, a number of reviews have been published which focus on methods for preparing MOF films,^[31-35] and the design and application of conductive MOFs.^[36-42] However, there has not been a comprehensive review of conductive MOF films and their applications. This article systematically reviews the latest research progress on conductive MOF films. It first reviews the main preparation methods for obtaining MOF films, then discusses the various strategies for introducing conductivity into MOFs, including using special organic ligands, introducing redox active molecules (e.g. TCNQ, I_2) and the introduction of conductive polymers (e.g. polypyrrole, polythiophene). Finally, the electrochemical applications of conductive MOF films are reviewed, including applications in electrochemical sensing, energy storage and energy conversion(**Figure 1**). This review will provide guidance for better understanding and tuning the design strategies to obtain continuous, smooth MOF films with controllable thickness, high quality and high conductivity.

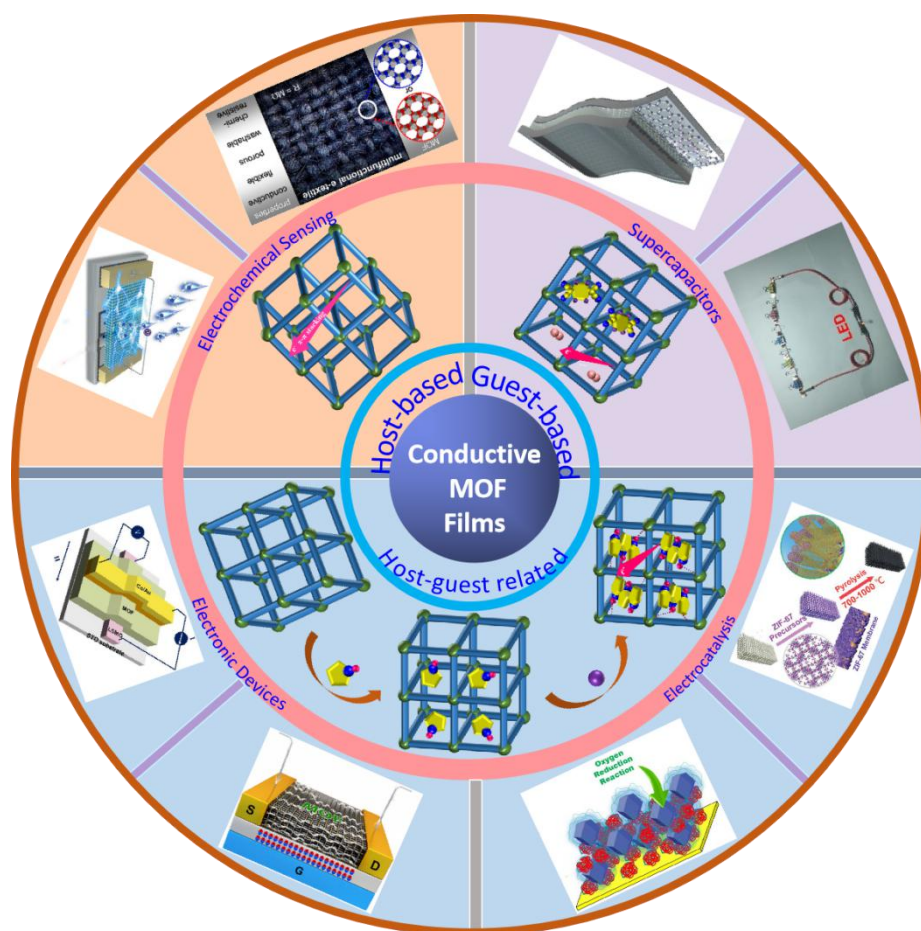


Figure 1. The main framework of the progress reports. Design principles of three conductive MOF films (Host-based, Guest-based, Host-guest related) and corresponding applications. Electrochemical sensing. Reproduced with permission.^[43] Copyright 2017, Wiley-VCH. Reproduced with permission.^[44] Copyright 2017, American Chemical Society. Supercapacitors. Reproduced with permission.^[45] Copyright 2013, Royal Society of Chemistry. Reproduced with permission.^[46] Copyright 2020, Elsevier. Electrocatalysis. Reproduced with permission.^[47] Copyright 2017, Wiley-VCH. Reproduced with permission.^[48] Copyright 2019, Royal Society of Chemistry. Electronic devices. Reproduced with permission.^[28] Copyright 2016, American Chemical Society. Reproduced with permission.^[30] Copyright 2019, Wiley-VCH.

2. Preparation of MOF Thin Films

2.1. Substrates for Preparing MOF Thin Films

Choosing suitable substrates and their surface modifications are key to preparing MOF films.

So far, many different types of substrates have been developed for MOF films deposition, including copper, silicon, silica, gold, aluminum, indium or fluorine doped tin oxide (ITO, FTO), and various polymers. The recently developed spray technology allows a continuous process with almost no restrictions on the size and type of substrate that can be used for the

MOF thin films preparation. However, among various preparation methods functionalization of the substrates is necessary, especially for the epitaxial growth of MOF films.

Due to the quite flexible nature of MOF thin films, many different methods depositing MOF films on solid substrates have been reported, which include liquid phase epitaxy, Langmuir-Blodgett layer-by-layer deposition, chemical vapor deposition, atomic layer deposition, interfacial synthesis and contra-diffusion synthesis. In this review, we divide these methods into two categories: (1) the solution-based preparation of MOF thin films, in which the substrates are immersed into a single or multiple solutions containing different reactants (including metal precursors and organic ligand precursors); (2) the vacuum preparation methods, in which MOF films are deposited on substrates using gaseous reactants under vacuum.

2.2. Solution-Based MOF Films Preparation Methods

2.2.1. Liquid Phase Epitaxy (LPE)

Among the many methods for preparing MOF films, liquid phase epitaxy is commonly applied to prepare porous, crystalline MOF films, also known as SURMOFs (surface anchoring, crystalline and oriented metal-organic framework multilayer). In this method, the two most critical factors for the deposition process are: (1) the functional substrate for the self-assembled monolayer (SAM) and (2) the alternating immersion of the substrate into solutions of metal ions and organic ligands to obtain the target MOF films.

This method is quite different from the traditional solvothermal method for the synthesis of MOFs, in which all reactants are uniformly mixed at a high temperature (between 70°C and 150°C). In liquid phase epitaxy, the reactants are separated, and the metal ions and the organic ligands are sequentially deposited onto substrate.^[49] For example, in the preparation of the conductive MOF $\text{Cu}_3(\text{BTC})_2$ (HKUST-1), a gold substrate is functionalized using 16-mercaptohexadecanoic acid (MHDA) and 11-mercaptoundecanol (MUD) to form the SAM. The organic precursor (1,3,5-benzocarboxylic acid, H_3BTC) and inorganic precursors

(copper(II) acetate, $\text{Cu}(\text{OAc})_2$ and $\text{Cu}(\text{NO}_3)_2$) are dissolved in ethanol in different beakers. The substrate is then sequentially immersed into the two solutions. Between each step, the substrate is cleaned with ethanol and then dried under nitrogen to remove excess adsorbate (**Figure 2a**). When the SAM is terminated by the $-\text{COOH}$ groups, the resulted film exhibits a [100] crystalline face, while when the SAM is terminated by the $-\text{OH}$ groups, the resulted film exhibits a [111] crystalline face. It is worth noting that LPE method is crucial to the selection of the metal composition for HKUST-1 SURMOF growth. When $\text{Cu}(\text{NO}_3)_2$ is used as metal ion precursor, almost no HKUST-1 growth is observed regardless of the orientation. While when $\text{Cu}(\text{OAc})_2$ is used, which has a molecular paddle wheel structure similar to the HKUST-1 metal node, the growth is smooth. Surface plasmon resonance spectroscopy (SPR) shows that as the number of alternating immersion cycles increases, the thickness of the film deposited on the substrate increases linearly,^[50] and multilayer films can be deposited stepwise via immersing an Au substrate in the ethanol solution of mercaptohexadecanoic acid (MHDA) to form a SAM on the surface of the substrate, and then adding $\text{Cu}(\text{OAc})_2$ and H_3BTC sequentially. Apart from MOF HKUST-1, other MOF films, such as $\text{Fe}(\text{py})_2[\text{Pt}(\text{CN})_4]$,^[51] MOF-508,^[52] were successfully prepared by the same method.

In 2015, Zhou *et al.* used four macroporous polymer films, polyethylene (PE), polypropylene (PP), polystyrene (PS), and polyvinylidene fluoride (PVDF), as the substrates for preparation of the MOF films.^[53] However, because these polymers have extremely low surface energies and surface tensions, MOF materials cannot be deposited on these inert polymers. A workaround was found by immersing these substrates in a weakly alkaline dopamine hydrochloric acid solution, which leads to the self-polymerization of dopamine, forming a firmly bonded polydopamine (PDA) film onto the surface of the polymer (**Figure 2b**). A dense PDA coating can be prepared on any type of solid surfaces and can serve as the nucleation sites for the MOF films. The HKUST-1, MIL-100(Fe), MOF-5, and ZIF-8 MOF films have been successfully prepared using a PDA film and the layer-by-layer deposition

method. The catechol group in PDA coating is a good ligand for metal ions, so it can be used to stabilize the metal ions to deposit a MOF thin film onto a substrate like PP.

Recently, many researchers have started to combine liquid phase epitaxy with other methods to prepare high quality films. For instance, Zhao *et al.* reported a combination of atomic layer deposition (ALD) and layer-by-layer deposition to prepare MOF HKUST-1 films on polymer substrates.^[54] First, atomic layer deposition is used to deposit a metal oxide (Al_2O_3) film with a controlled thickness on a non-woven fiber mat, and then the MOF film is prepared onto the metal oxide coated surface of the substrate by layer-by-layer deposition (**Figure 2c**). The number of processing cycles controls the thickness of the resulting film. Here, the metal oxide layer serves as the nucleation layer for the MOF film and promotes the growth of the MOF film. As can be seen from the figure, the PP fiber without an Al_2O_3 coating shows uneven and irregular MOF growth, while the MOF growth on the PP@ALD fiber is uniform and smooth. Pure PP fibers do not contain reactive functional groups and are relatively inert to MOF nucleation. However, MOF nucleation may occur on the surface defects of the substrate. Once the nucleation seed attaches to the untreated fiber, the MOF will preferentially grow at that location.

In 2016, Eddaoudi *et al.* successfully developed a simple MOF thin film growth method by combining spin coating with liquid phase epitaxy.^[55] The method overcomes the shortcomings of the traditional liquid phase epitaxy method, including its long production process, high cost and the difficulty of scaling up production, and prepares poly-crystalline MOF films with a high degree of orientation, high crystallinity and good uniformity. During the preparation process, a fully automatic rotating coater with 4 miniature syringes, is used for the coating process. First, the metal ion solution is dropped from a syringe and the solution evenly coats the whole substrate surface as the device rotates. Afterwards, solvent is injected into the syringe to wash the substrate. Next, the organic ligand solution is dropped from a syringe, and finally the substrate is washed with a solvent. These four steps compose a

reaction cycle and the thickness of the MOF film is controlled via adjusting the reaction cycles. HKUST-1, ZIF-8 and $\text{Cu}_2(\text{bdc})_2 \cdot x\text{H}_2\text{O}$ thin films have been successfully prepared using this method.

Recently, Xu *et al.* for the first time combined a spray method with liquid phase epitaxy.^[43] $\text{Cu}(\text{OAC})_2$ and the organic ligand 2,3,6,7,10,11-hexahydroxytriphenylene (HHTP) were used as the two precursors to prepare a $\text{Cu}_3(\text{HHTP})_2$ conductive MOF(EC-MOF) film with high crystallinity, a high degree of orientation and a smooth surface on an -OH functionalized substrate (**Figure 2d**). The thickness of the film increased by ~2 nm on average during each growth cycle, allowing precise control of the growth of the film. The obtained MOF film is dense and continuous and has excellent sensing performance at room temperature. Although the liquid phase epitaxy method can effectively control the thickness and the orientation of deposited film, it is not suitable for the formation of all types of MOF films.

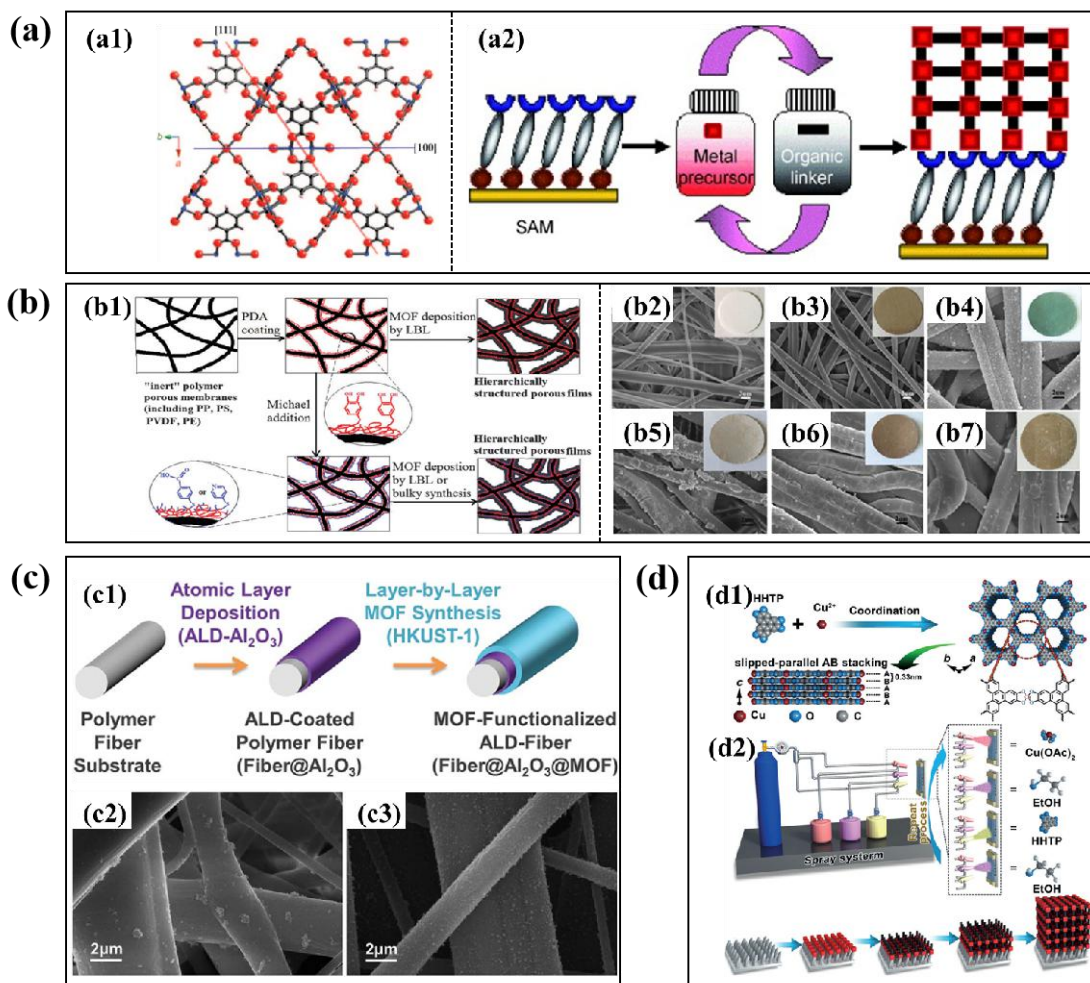


Figure 2. Preparation of MOF films by LPE. a) HKUST-1 MOFs film. a1) Schematic diagram of the structure of HKUST-1. a2) Sketch map of the gradual growth of SURMOFs on a SAM- functionalized substrate. The method includes repeated cycles of immersing into a metal precursor solution and an organic ligand solution, and cleaning the material with a solvent in an intermediate step. Reproduced with permission.^[49] Copyright 2009, Wiley-VCH. (b) b1) Schematic diagram of the production process of MOF-modified PP membranes. b2)~b7) SEM images of an original PP fiber membrane, a PDA-modified PP membrane, and a PP membrane with various deposited MOFs. Reproduced with permission.^[53] Copyright 2015, Royal Society of Chemistry. (c) c1) Schematic diagram of the synthesis process. c2, c3) SEM micrographs of MOF film after 20 growth cycles on untreated and treated PP substrates. Reproduced with permission.^[54] Copyright 2015, Royal Society of Chemistry. (d) d1) Cu₃(HHTP)₂ crystal structure. d2) Preparation of a Cu (HHTP) thin film gas sensor. Reproduced with permission.^[43] Copyright 2017, Wiley-VCH.

2.2.2. Langmuir-Blodgett Layer-by-Layer Deposition

The Langmuir-Blodgett (LB) method is a feasible method for the preparation of ordered nanosheets with large areas on a liquid surface (**Figure 3a**).^[56] Dispersing the monomers of the two-dimensional materials on the liquid surface forms a dense film, resulting in the deposition of single-layer nanosheets on the substrate when the metal ion solution is added.^[57]

In recent years, researchers have often combined the layer-by-layer method with the LB method to prepare very flat, uniform, ordered and oriented MOF thin films on solid surfaces.^[34] H. Kitagawa *et al.* prepared a perfect MOF nanofilm (NAFS-1) composed of metalloporphyrin building units with preferential orientation on a solid surface at room temperature.^[58] As shown in the **Figure 3b**, NAFS-1 is a two-dimensional array formed by interconnected cobalt-containing porphyrin units (CoTCCP) and dual-core copper paddle wheel units. First, the metal ion and ligand- containing solution is compressed by the LB method, and then 2D layered MOF sheets are fabricated on the surface of aqueous solution. And the two-dimensional array is deposited on the upper surface of the substrate under room temperature via the horizontal immersion. Finally, the gradual growth of target MOF film to the desired thickness is achieved by repeatedly transferring 2D MOF flakes onto the substrate.

NAFS-2, which has a structure similar to NAFS-1, was also prepared using this method (**Figure 3c**).^[59] The main difference between NAFS-2 and NAFS-1 is that there is no pyridine ligand in the NAFS-2 axial position, and the porphyrin cage is empty. And the most important advantage of the method is that supporting units between the layers are not required, which makes the distance between the layers adjustable and makes it possible to construct an ordered nanofilm outside and inside the plane.

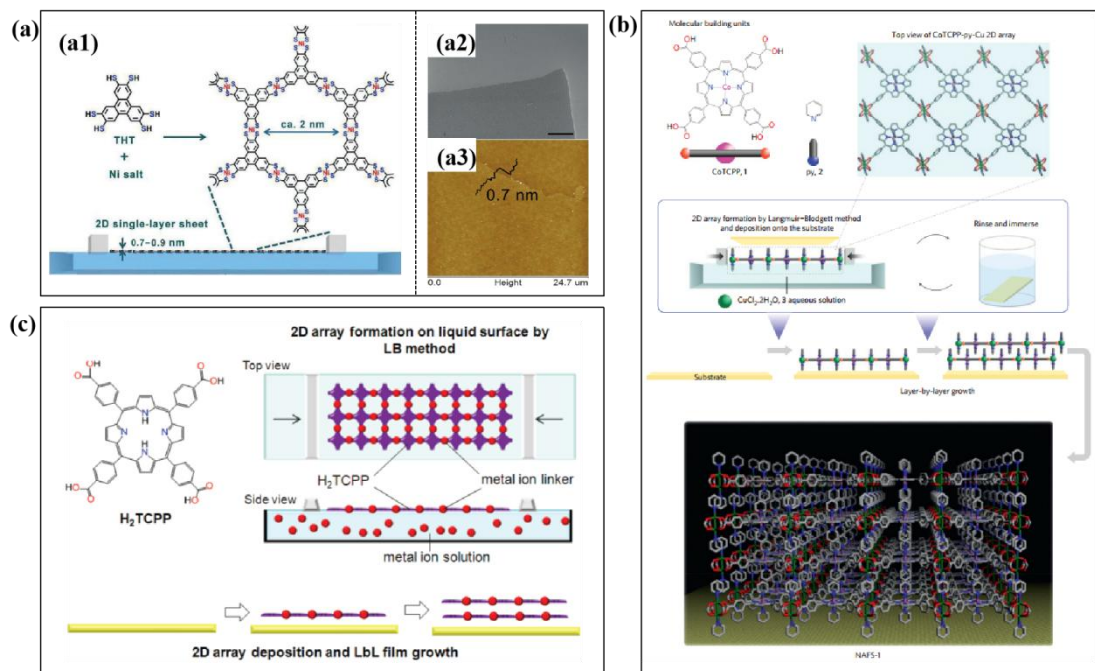


Figure 3. a) a1) Synthetic schematic diagram of a triphenylene-fused nickel bis(dithiolene) complex. a2) SEM image of a single-layer sheet. a3) AFM height scan. Reproduced with permission.^[56] Copyright 2015, Wiley-VCH. b) Schematic diagram of NAFS-1 manufacturing method. Reproduced with permission.^[58] Copyright 2015, Nature. c) Schematic diagram of the preparation process of NAFS-2. Reproduced with permission.^[59] Copyright 2011, American Chemical Society.

2.2.3. Interface and Contra-Diffusion Synthesis

In contrast to the two methods mentioned above, the interfacial and reverse diffusion synthesis involve the separation of the two metal reactant and ligand solutions by the substrate (contra-diffusion synthesis) or through the interface of two insoluble solvents (interfacial synthesis). Different interfacial synthesis approaches for preparing MOF films include the liquid-liquid interface synthesis, which usually occurs at the interface of two insoluble solutions, and gas-liquid interface synthesis, which is carried out at a gas-liquid interface through the coordination effect of metal ions and ligands.

Liquid-liquid Interface Synthesis

Ameloot *et al.* firstly presented the use of liquid-liquid interface method to prepare the MOF films.^[60] They used this method to synthesize three-dimensional hollow capsules. During the preparation process of $\text{Cu}_3(\text{BTC})_2$ film, $\text{Cu}(\text{OAc})_2 \cdot \text{H}_2\text{O}$ was added to the water with 1-4 wt% PVA to obtain the aqueous phase, which was injected via a hollow needle into the organic

ligand solution (H_3BTC dissolved in the 1-octanol) flowing via a polytetrafluoroethylene tube. The resulting solution was used to prepare the $\text{Cu}_3(\text{BTC})_2$ film. The difference in solubility between the organic and inorganic precursors brought about the automatic formation of the MOF layer in the phase segregated reaction mixture. The nucleation and growth of the $\text{Cu}_3(\text{BTC})_2$ film takes place at the interface of the solution, where the two precursors come into contact with each other.

To prepare a two-dimensional layered conductive Cu-BHT film at a $\text{CH}_2\text{Cl}_2/\text{H}_2\text{O}$ interface, Zhu *et al.* used a liquid-liquid interface method adapted from the method used for the preparation of Ni-BHT complexes (**Figure 4a**).^[61,62] After transferring the films to a substrate, continuous thin films larger than 1 cm^2 were obtained. It is worth noting that the two sides of the thin films showed different morphologies. On the upper surface, the films were flat with little roughness, and were relatively continuous on a large scale, while on the lower surface the stacking was looser and the surface was rougher due to the random orientation of the plate-like nano flakes.

However, the liquid-liquid interfaces are mainly generated between insoluble organic/aqueous phases or organic/organic phases. Due to the inhomogeneity of nucleation, it is difficult to adjust the thickness and orientation of the prepared MOF films.^[63] In 2018, Bai *et al.* used a spray-assisted mixed-phase liquid-liquid interfacial synthesis strategy to quickly and controllably prepare an free-standing CuBDC MOF film with a large area at room temperature.^[64] The resulting film was uniform and compact, and had good mechanical flexibility (**Figure 4b**). This is mainly due to two key factors. The first is the choice of a suitable solvent. The DMF was used as the reaction solvent and the CH_3CN was used as a co-solvent to form a stable mixed liquid-liquid interface. The crystals grew dominantly in lateral direction, without additional longitudinal growth, in order to obtain CuBDC nanosheets. And the second key factor is the spraying method. The solution is dispersed into tiny droplets, reducing the interference with the interface upon contact with the other phase, and avoiding

the diffusion that occurs during the direct mixing of the DMF and CH_3CN . With slow addition, the liquid-liquid interface can be maintained for a long time.

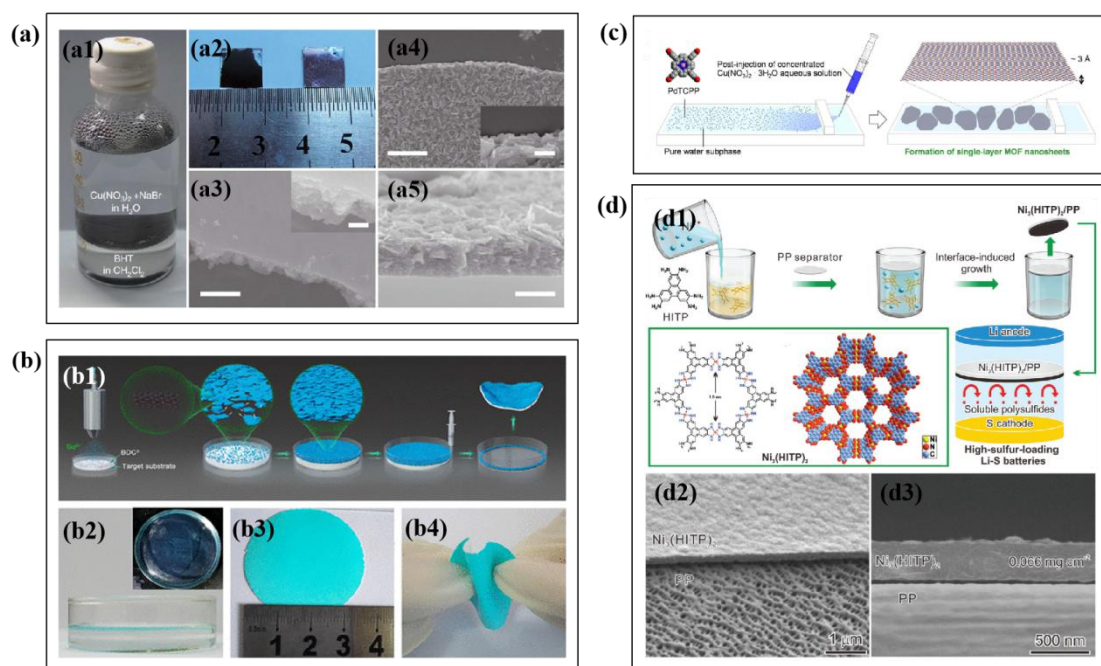


Figure 4. a1) Photograph of a Cu-BHT film. a2) Upside up (right) and upside down (left) film photographs transferred on a glass substrate. a3, a4) SEM images of the upper and lower surfaces. a5) Cross-section part of a 200 nm thick film. Reproduced with permission.^[62] Copyright 2015, Nature. b1) Schematic diagram of the preparation of a CuBDC thin film. b2) Photo of a CuBDC free-standing film. b3, b4) Photograph of CuBDC/hydrophobic filter composite membrane. Reproduced with permission.^[64] Copyright 2018, American Chemical Society. c) Schematic diagram of the NAFS-13 nanosheet preparation process. Reproduced with permission.^[65] Copyright 2013, Nature. d1) Schematic diagram of the application of the conductive $\text{Ni}_3(\text{HITP})_2$ modified separator grown on the interface in Li-S batteries. d2, d3) Cross-section SEM images of a $\text{Ni}_3(\text{HITP})_2$ membrane. Reproduced with permission.^[66] Copyright 2018, Wiley-VCH.

Gas-Liquid Interfacial Synthesis

Similar to liquid-liquid interfacial synthesis, the gas-liquid interfacial synthesis method is another excellent platform for assembling two-dimensional sheets of materials. In 2013, Makiura et al. proposed a gas-liquid interfacial strategy to prepare two-dimensional molecular crystalline MOF nanosheets consisted of the porphyrin building units connected by the metal ions (NAFS-13).^[65] During the preparation process, a solution of the molecular building unit PdTCPP is directly diffused on a subphase of pure water, and then a $\text{Cu}(\text{NO}_3)_2 \cdot 3\text{H}_2\text{O}$ solution is slowly injected into the subphase from side surface, which is shown in **Figure 4c**.

Compared with a traditional synthesis method, the NAFS-13 nanosheets, prepared using this post-injection method, exhibits a smoother sheet-like morphology. Due to the slow injection growth the area of the flakes expands at the microscopic level, while providing a smooth surface morphology of the monomolecular flakes at the macroscopic level.

In 2016, Xu *et al.* successfully prepared an independent MOF film with a smooth and dense surface using the gas-liquid interface self-assembly process.^[30] They completely mixed HATP•6HCl (HATP = 2,3,6,7,10,11-hexaaminotriphenylene) and NiCl₂•6H₂O, heated the reaction mixture to 60°C and afterwards added trimethylamine (Et₃N). The formation of the MOF film occurs at the gas-liquid interface, and it is visible to the naked eye. Then, the prepared MOF film is transferred to a SiO₂/Si wafer substrate via stamping process. Thickness of the film can be adjusted via controlling the specific reaction time. After 3 min of reaction, the film obtained thickness is 100 nm, and the color of the film intensifies with increasing thickness eventually becoming dark blue.

In 2017, Xu *et al.* applied the same gas-liquid interface strategy to manufacture a free-standing microporous Ni₃(HITP)₂ thin film with a large area, smooth surface, and controllable thickness.^[66] During the preparation process, the metal ion solution and the organic ligand solution are mixed before placing a PP separator on the surface of the solution. Finally, a PP separator coated with a Ni₃(HITP)₂ film is obtained (**Figure 4d**). The PP separator, modified with Ni₃(HITP)₂, has good mechanical properties. The film also shows strong adhesion and is not easily separated from the substrate. The Ni₃(HITP)₂ film and PP can be separated using a blade. From the SEM image, it is clearly shown that the original PP separator has a highly porous structure and different pore size distribution. The dense microporous Ni₃(HITP)₂ layer completely covers the surface of the PP separator, and the thickness of MOF film can be adjusted by controlling the specific reaction time.

Contra-Diffusion Synthesis

In order to achieve good MOF film growth, it is essential to achieve heterogeneous nucleation of the MOF on a substrate. Many strategies have been developed for this, including modifying the substrate surface and adding seed crystals to the substrate. However, these strategies often complicate the film synthesis process. This not only raises the manufacturing cost of the film, but also often results in films with poor microstructures. Yao *et al.* presented a new method for the preparation of the ZIF-8 films, directly on both sides of the nylon substrate, using the contra-diffusion synthesis.^[67] This strategy uses a porous nylon membrane to separate the different reactant solutions and the crystallization of ZIF-8 on surface of the membrane is due to the reverse diffusion of the solution. As shown in **Figure 5a**, solutions of 2-methylimidazole (Hmim) and zinc nitrate are put on different sides of the nylon membrane. The two solutions diffuse in opposite directions from both sides of the nylon membrane, forming ZIF-8 films on both sides of the membrane. On the zinc nitrate solution side, cubic crystals can be observed. As the crystallization time increases, the size of the ZIF-8 crystals gradually increases. While on the other side (Hmim), ZIF-8 nanoparticles grow around the fibrous structure of nylon matrix, but no continuous film. Huang *et al.* applied the same strategy to prepare a ZIF-71 film on an inorganic hollow fiber substrate that had good alcohol-water pervaporation separation performance (**Figure 5b**).^[68]

Jeong *et al.* synthesized a high-quality ZIF-8 film on a self-made α -Al₂O₃ disk using an *in situ* synthesis strategy derived from the reverse diffusion.^[69] The preparation process is shown in **Figure 5c**. First, the disk is placed in the metal ion precursor solution, and then the saturated disk is placed vertically in a hydrothermal kettle containing the ligand solution, where it undergoes a solvothermal reaction. The interdiffusion of the metal ions and ligand leads to the formation of "reaction zone" at the interface. And the MOF quickly nucleated near the interface, forming a well-grown and continuous ZIF-8 film. The membrane had good performance for separating a mixture of propylene/propane, and the separation capacity of the

resulted ZIF-8 film remained high after 2 h of intense ultrasonication. When using the contra-diffusion method to prepare MOF films, the thickness of the film can be regulated by adjusting the specific reaction time and the ratio of metal ions and organic ligands in the reaction.^[70]

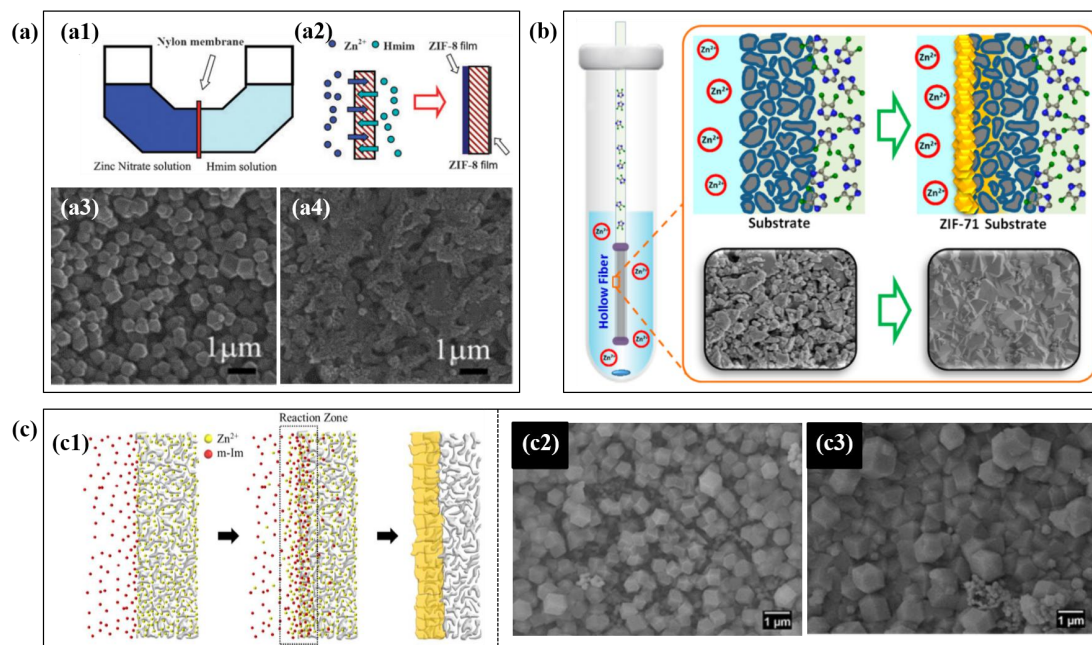


Figure 5. a1) Preparation of diffusion cells for ZIF-8 film. a2) Schematic diagram of the formation of a ZIF-8 film. SEM images of a ZIF-8 film on the side of a3) the zinc nitrate solution and a4) the Hmim solution prepared on nylon membrane. Reproduced with permission.^[67] Copyright 2011, Royal Society of Chemistry. b) Schematic of the preparation of a ZIF-71 hollow fiber film. Reproduced with permission.^[68] Copyright 2015, American Chemical Society. c1) Schematic diagram of the *in situ* preparation of a ZIF-8 film. c2) and c3) SEM images of ZIF-8 film grown for 2 min and for 30 min. Reproduced with permission.^[69] Copyright 2013, American Chemical Society.

2.2.4. Growth from Solvothermal Mother Solutions

In Situ Growth

The solvothermal synthesis is also a simple and effective method for preparing various MOF films. A stainless steel autoclave, lined with polytetrafluoroethylene (PTFE), is the main piece of equipment used for this type of synthesis. The reactant solubility and reactivity are improved by the high temperature and high pressure generated in the solution, so that the MOF crystal nucleation and the growth process are uniform. The most direct method for preparing MOF films is to prepare MOF mother solutions with a given ratio, and then insert

one or more substrates into the solution. The crystal growth occurs on the surface of the substrate, and sometimes in the solution, which causes the resulted crystals to stick to the surface of substrate via a relatively symbiotic and continuous fashion. Many MOF films have been prepared using this method. Ho *et al.* grew a MOF-525 film on a conductive glass substrate using the solvothermal method.^[71] Afterwards, the films were post-metallized with ZnCl₂ and CoCl₂ solutions to obtain Zn-MOF-525 and Co-MOF-525 films, respectively (**Figure 6a**). The obtained films are composed of uniformly distributed MOF-525 cubic crystals with sizes ranging from 500-1000 nm, and the crystals are embedded in each other and evenly attached to the FTO substrate. The post-metallized film retains the morphology and crystallinity of original MOF film, and all these films exhibit electrical activity in aqueous media. Shah *et al.* synthesized a well-interlaced continuous ZIF-8 membrane on an α -Al₂O₃ substrate by *in situ* solvothermal method.^[72] α -Al₂O₃ was placed in a mixed solution of zinc chloride (ZnCl₂), sodium formate and 2-methylimidazole (mIm), and heated to 120°C to undergo the solvothermal reaction and a continuous and dense ZIF-8 film with the thickness of ~25 μ m was successfully synthesized. In addition, the same strategy was applied to synthesize several other continuous ZIF films, such as ZIF-7, Zn(Im)₂ (similar to ZIF-61), ZIF-90 and SIM-1, demonstrating the universal applicability of this strategy.

The same growth strategy was used by Li *et al.* to prepare a new type of porous [Co₃(TBTC)₂(DMF)₂] \cdot 4DMF MOF thin film on an α -Al₂O₃ substrate.^[73] And, the substrate is activated at different temperatures before immersion into the mother solutions for solvothermal growth. As the activation temperature increases, the crystals transform from an initial cone shape to thin flakes (**Figure 6b**). At higher pre-activation temperatures, the films become denser and the grain sizes smaller. This is mainly due to the fact that the pre-activation temperature enhances the surface activity of the alumina matrix and changes the density of its surface hydroxyl groups, thereby increasing the nucleation density. Thus, the surface properties of the substrate have significant influence on the growth of the MOFs.^[74]

Solvothermal methods have been previously used to prepare MOF films, but the resulting films were thick and randomly orientated, which limited their application in membrane separation. Therefore, Miyamoto et al. prepared UiO-66 films on the silicon substrate using an *in situ* solvothermal synthesis.^[75] A highly oriented UiO-66 film with a single crystal layer was formed via adding acetic acid and water during the synthesis. The prepared UiO-66 film is composed of octahedral crystals. Among the dense region, the film surface is very smooth with few grain boundaries, but in other regions the grain boundaries are larger. After three rounds of solvothermal treatment, a film with a thickness consistent with the monocrystalline silicon layer was prepared. Thus, repeated solvothermal treatment promotes the nucleation process of UiO-66, instead of further crystal growth of the already-formed crystal.

Recently, many studies have combined atomic layer deposition (ALD) with solvothermal methods to prepare high-quality MOF films on polymer substrates. Jr et al. first deposited TiO₂ coatings (using TiO₂ as a nucleation site for MOF growth) on different polymer fiber substrates (including PP, polyamide-6 (PA-6), PVDF/Ti(OH)₄, and poly(methylmethacrylate) (PMMA)/Ti(OH)₄) by ALD, and then UiO-66-NH₂ MOF films were synthesized on the TiO₂-coated substrates using a solvothermal method.^[76] It is shown that the differences in the chemical stability and physical stability of the polymer fiber matrix under the MOF synthesis conditions leads to differences in the structure and properties of the final composite.

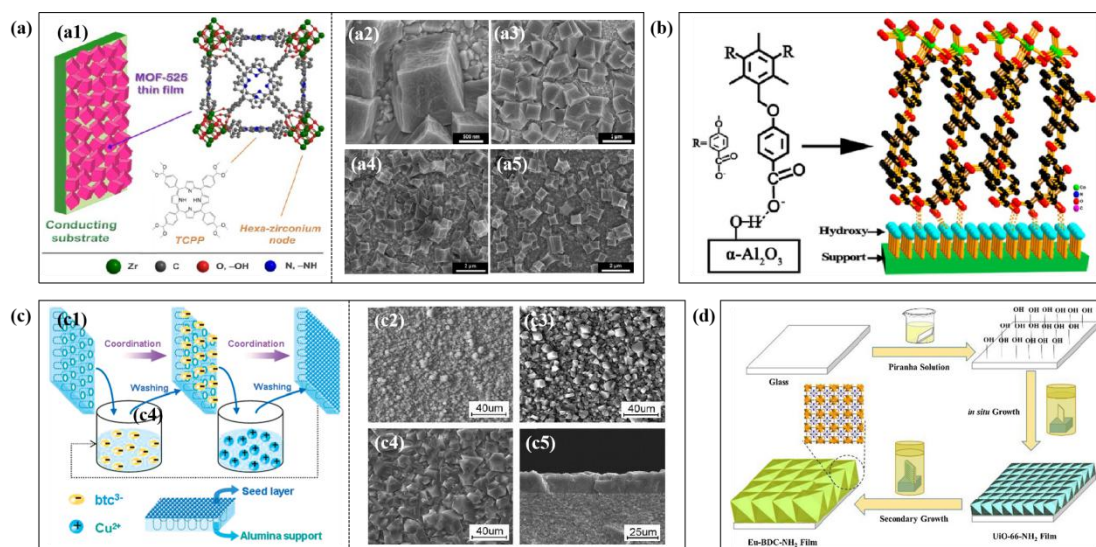


Figure 6. a) Schematic diagram of the MOF-525 film structure. a2, a3) SEM images of MOF-525 film under different magnifications and SEM images of a4) Zn-MOF-525 film, a5) Co-MOF-525 film. Reproduced with permission.^[71] Copyright 2012, Royal Society of Chemistry. b) The growth of $[\text{Co}_3(\text{TBTC})_2(\text{DMF})_2] \cdot 4\text{DMF}$ on $\alpha\text{-Al}_2\text{O}_3$ substrates. Reproduced with permission.^[73] Copyright 2013, American Chemical Society. c) Schematic diagram of BTC^{3-} and Cu^{2+} on a alumina substrate. c2, c3, c4) SEM images of surface of HKUST-1 membranes prepared with three different synthesis solutions: (I) 0.01 M H_3btc + 0.015 M $\text{Cu}(\text{NO}_3)_2 \cdot 3\text{H}_2\text{O}$; (II) 0.02 M H_3btc + 0.03 M $\text{Cu}(\text{NO}_3)_2 \cdot 3\text{H}_2\text{O}$; (III) 0.04 M H_3btc + 0.06 M $\text{Cu}(\text{NO}_3)_2 \cdot 3\text{H}_2\text{O}$ and c5) the cross section of c4). Reproduced with permission.^[79] Copyright 2011, American Chemical Society. d) *In situ* secondary growth procedure of an Eu-BDC-NH₂ film on a glass support. Reproduced with permission.^[80] Copyright 2018, Elsevier.

Seed-Assisted Growth

Seed-assisted growth, also known as the secondary growth, is a commonly used method. The process involves two steps: first, the seed layer is deposited on the substrate, and then the MOF film is grown using a hydrothermal or solvothermal method. Due to the low heterogeneous nucleation density of numerous MOFs on the porous ceramic substrates, this strategy is becoming more and more popular for the preparation of MOF films. Various seed layers can be used, including MOF nanocrystals, coordination polymers or MOF films.^[77]

In 2009, Tsapatsis *et al.* applied the seed-assisted growth method to prepare a microporous MOF films with preferential orientation and good growth dynamics on porous $\alpha\text{-Al}_2\text{O}_3$ substrates.^[78] During the preparation process, the substrate is modified with polyethyleneimine (PEI) to enhance the adhesion of the seed layer. Independently, a MOF solution with a specific ratio is prepared and undergoes a solvothermal reaction at 150°C to

form seed crystals. The MOF crystals that form are manually assembled and deposited on the modified substrate as a seed layer. Although the coverage of the substrate is complete, the seed crystals are not tightly packed due to their uneven particle shape and size. Finally, the substrate coated with the seed layer is placed into the same solution that was used for the seed crystal synthesis and heated to obtain a continuous MOF films with a thickness of $\sim 20 \mu\text{m}$. Due to competitive growth of the seeds during this secondary growth process, a randomly oriented seed layer is deposited to form an oriented film.

Jin *et al.* developed a method for using a coordination polymer as the seed layer and *in situ* growing the MOF films on it.^[79] They first deposited 4 cycles of Cu^{2+} and btc^{3-} on a porous alumina disk using a layer-by-layer deposition method, and then a $\text{Cu}_3(\text{BTC})_2$ MOF film was grown *in situ* using a solvothermal method (**Figure 6c**). During the growth of the $\text{Cu}_3(\text{BTC})_2$ film, the integrity and continuity of the film can be adjusted by regulating the reactants concentrations. And a continuous and highly symbiotic $\text{Cu}_3(\text{BTC})_2$ film is obtained at higher reactant concentrations.

Recently, Qian *et al.* applied the same strategy, called *in situ* secondary growth, to prepare an Eu-BDC-NH₂ MOF film on a glass substrate using a UiO-66-NH₂ film as the seed layer (**Figure 6d**).^[80] The glass substrate is modified with a hydroxyl-containing solution to attach active groups on the surface, and then the modified substrate is placed in the prepared MOF solution. A solvothermal reaction is performed to obtain a glass substrate covered with UiO-66-NH₂ film, which is used as the seed layer. Then a second solvothermal reaction is performed to obtain the Eu-BDC-NH₂ MOF film. Due to similar crystal structures and identical ligands in UiO-66-NH₂ and Eu-BDC-NH₂, a Eu-BDC-NH₂ film can be perfectly prepared by *in situ* secondary growth on the UiO-66-NH₂ layer.

2.2.5. Electrochemical Deposition

Electrochemical deposition method has been widely used in the preparation of MOF films due to its advantages of simple operation, mild reaction conditions, continuous large-scale

production, and no harm to the environment.^[81] Müller *et al.* proposed for the first time to prepare HKUST-1 MOF thin films by electrochemical deposition.^[82] Since then, researchers have carried out a large amount of research on the preparation of high-quality MOF films by electrochemical method.^[83,84] Generally speaking, there are three different methods to prepare MOF films by electrochemical methods, including the anodic deposition, electrophoretic deposition and cathodic deposition.

In the anodic deposition process, the anode electrode is electrochemically oxidized to release metal ions. When the electrochemically generated metal ions react with the organic ligands in the electrolyte, the MOF film is formed on the anode surface (**Figure 7a**). Oliver *et al.* also deposited HKUST-1, $[\text{Cu}(\text{C}_{10}\text{H}_8\text{N}_2)^{2+}]\text{Br}_2$ and Zn-BTC, Zn-BPDC electrochemical MOF (EMOF) films on Cu-ITO and Zn-ITO by anodic deposition, respectively.^[85] The size and coverage density of the deposited crystals can be adjusted by changing the voltage, the time of applying the bias voltage and the solution concentration. Anodic electrochemical deposition method has also been widely used to prepare various types of MOF films on metal substrates, including $\text{Cu}_3(\text{BTC})_2$ on Cu electrodes,^[86] MIL-100 on Fe anodes,^[87] and $\text{Zn}_3(\text{BTC})_2$ on Zn plates,^[88] $[\text{Zn}(\text{TBTC})] \cdot 2\text{DMF} \cdot \text{EtOH}$ on the Zn plates.^[89]

Herein, another method of electrophoretic deposition (EPD) is also a well-established technique for fabricating MOFs thin films. By immersing the two electrodes in the solution containing the MOF particles for the deposition, when a voltage is applied between the two electrodes, the electric field generated will drive the target MOF particles to approach the electrode with opposite charge and form MOF film on the electrode, as shown in the **Figure 7b**. Hupp *et al.* successfully prepared four representative MOF films, including HKUST-1, AL-MIL-53, UiO-66 and NU-1000 on conductive fluorine doped tin oxide (FTO) substrates via the electrophoretic deposition process.^[90] HKUST-1 and ZIF-8 films were also successfully prepared on the porous stainless steel by Zhu *et al.*^[91]

Dincă *et al.* firstly reported the preparation of MOF film by the method of cathodic deposition.^[92] In this process, inert electrodes (working electrode and counter electrode) are used as the chemical inert separators. They are only used as electron sources and do not participate in the formation of MOF film. The key step of cathode deposition process is to obtain the local alkaline region of deproton of organic ligands near the cathode. The deproton organic ligands react with metal precursors in solution, causing the MOF particles to crystallize on the cathode surface to form a MOF film. Then, in 2014, Dincă group successfully prepared MOF-5, $Zn_4O(BDC)_3$ films under different voltage conditions *via* this method, as shown in the **Figure 7c**.^[93]

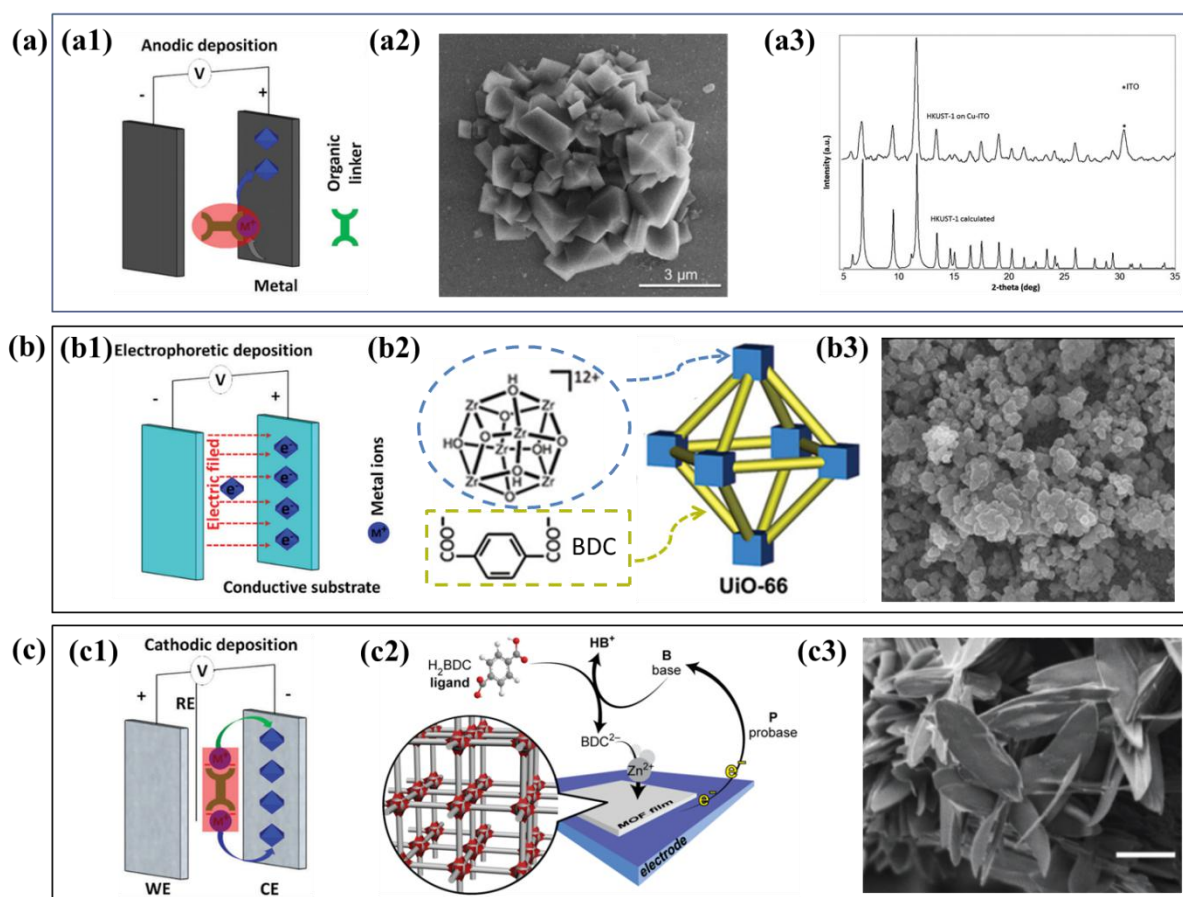


Figure 7. Schematic diagram of electrochemical preparation of MOF film by (a1) anodic deposition. (b1) electrophoretic deposition. (c1) cathodic deposition. Reproduced with permission.^[63] Copyright 2017, Royal Society of Chemistry. a2,a3) SEM image of the surface covered by HKUST-1 MOF crystal and its corresponding GIXRD after anodic deposition at 0.75 V on Cu-ITO for 50 minutes. Reproduced with permission.^[85] Copyright 2019, American Chemical Society. b2) Schematic diagram of the crystal structure of UiO-66 MOFs. b3) SEM image of UiO-66 film deposited by electrophoretic deposition. Reproduced with permission.^[90] Copyright 2014, Wiley-VCH. c2,c3) Schematic diagram of the structure of

MOF-5 prepared by cathode deposition and its corresponding SEM image of MOF-5 film. Reproduced with permission. ^[93]Copyright 2014, Royal Society of Chemistry.

2.3. Vacuum-Based MOF Films Preparation Methods

Most of the published methods used for the synthesis of MOF films usually involve the chemical reactions in organic solvents. However, these solution-based preparation methods can lead to contamination of the MOF films by the solvent, affecting the morphology and quality of the films. As a result, for avoiding the disadvantages of solution-based methods, various vacuum-based methods for the preparation of MOF films have been reported, such as chemical vapor deposition (CVD) and atomic layer deposition (ALD).

2.3.1. Chemical Vapor Deposition

CVD includes all vapor deposition processes that involve the rearrangement of chemical bonds to form a uniform thin film with precisely controlled thickness through the reaction of evaporated substances on or near the substrate. The advantage of CVD is that the vapor pressure of the precursor does not directly affect the properties of the deposited material.^[94] The first work about the preparation of MOF thin films using CVD (MOF-CVD) showed that the deposition process of ZIF-8 film is divided into two steps: (1) a ZnO precursor layer with a controllable thickness is deposited via ALD, and (2) the ZnO layer reacts with 2-methylimidazole (HmIm) vapor to form ZIF-8 film.^[95] Stassin et al. used this strategy to prepare a uniform MAF-6 ($[\text{Zn}(\text{eIm})_2]$) film with a mesoporous structure and a controllable thickness (**Figure 8a**).^[96] The morphology of the MAF-6 thin films synthesized using this method ranged from almost continuous to films consisted of dispersed micron-sized crystals. The high-resolution cross-sectional SEM image shows residual ZnO below the film, and the energy dispersive X-ray spectroscopy (EDS) showed that there was no residual Zn near the crystal. The thinner the ALD-ZnO layer is, the faster the ZnO layer is consumed, and the faster the MOF crystal matures. Ameloot *et al.* also performed studies using MOF-CVD.^[97] Their use of MOF-CVD generally includes two steps: (1) using physical vapor deposition to

deposit Cu or CuO films on silicon or glass substrates as a metal source, and (2) using a solid-gas reaction to deposit H₂BDC and H₂CDC on it. This forms CuCDC and CuBDC films with out-of-plane orientations and uniform porosity.

The most recent study of the preparation of MOF films by CVD was published by Li et al.^[98] They used steam-assisted CVD to grow a ZIF-67 film with high crystallinity on c-sapphire substrates (**Figure 8b**). During the synthesis, the metal precursor is first placed into a porcelain boat located in the center of the main heating furnace, and the ligand precursor is placed into another furnace located in the upstream zone. The substrate is placed in the downstream area next to the metal precursor. The steam from the two precursor solutions is carried to the substrate by a flow of mixed Ar/H₂O gas. This process results in a highly oriented ZIF-67 film on the substrate. The results show that the presence of water plays a decisive role in triggering the gas phase reaction. A highly oriented ZIF crystal can be obtained by changing the crystal growth and nucleation rate. In addition, the full vapor phase reaction environment and lower temperature growth conditions created by the steam-assisted CVD have significant potential for preparation and application of MOF films.

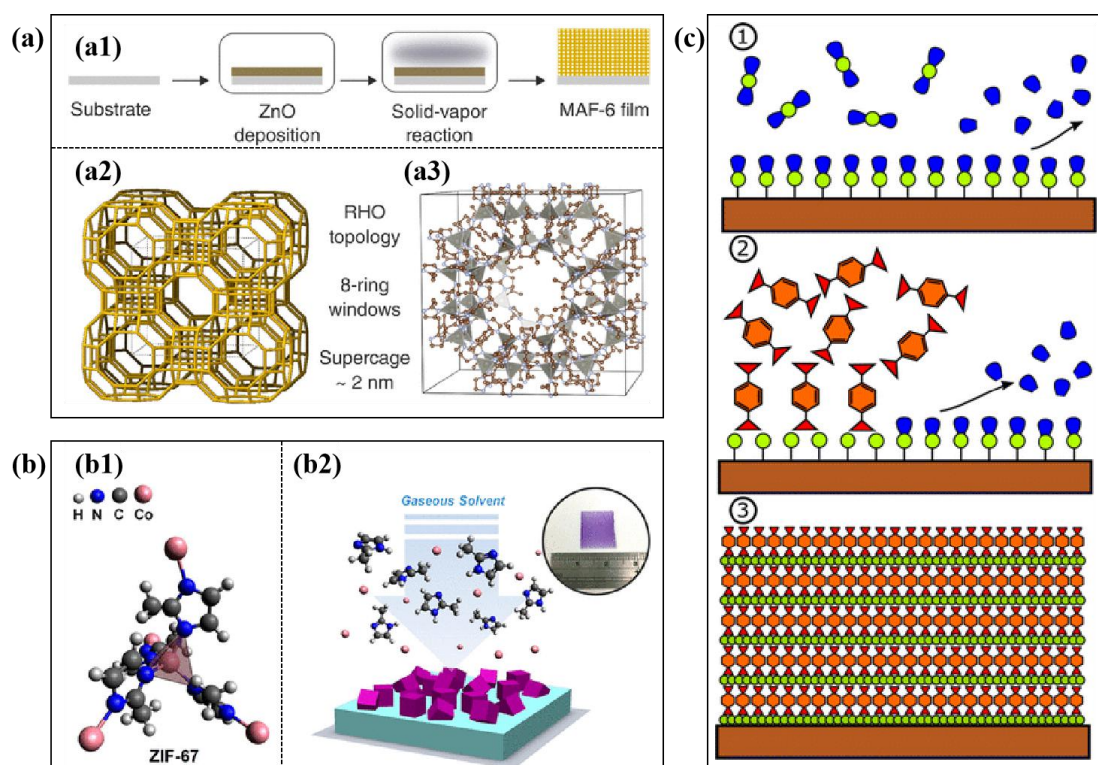


Figure 8. a1) Schematic diagram of the CVD process of MAF-6 film. a2) The MAF-6 RHO topology. a3) the cubic unit cell of MAF-6. Reproduced with permission.^[96] Copyright 2020, American Chemical Society. b1) Schematic diagram of the ZIF-67 structure. b2) Schematic diagram of the vapor deposition process of ZIF-67. Reproduced with permission.^[98] Copyright 2020, American Chemical Society. c) Schematic diagram of an ALD/MLD process for Ca-TP MOF film. Reproduced with permission.^[102] Copyright 2016, American Chemical Society.

2.3.2. Atomic Layer Deposition

ALD is another important technique for preparing MOF thin films under vacuum, and is a special form of CVD.^[99] The two precursors are supplied to the substrate surface using gas phase pulses, to produce ultra-thin and uniform MOF films. Any excess precursor is removed by the inert gas. This self-limiting growth process generates highly conformal films. The thickness of the film is controlled at the atomic or molecular level.

Karppinen *et al.* reported the use of terephthalic acid (TPA) as an organic precursor to directly prepare highly crystalline Cu-TPA MOF films on Si(100) substrates by ALD/MLD.^[100] During the preparation process, Cu(THD)₂ and TPA were used as precursors, and their sublimation temperatures were set to 110°C and 180°C, respectively. Uniform and conformal MOF coatings were fabricated on various substrate surfaces and device structures in a highly controllable manner. However, the temperature range required for the MOF formation (180-190°C) was relatively narrow in this study. Meanwhile, Salmi *et al.* successfully prepared MOF-5 thin films on silicon substrates by ALD, in which the ZnAc₂ and 1,4-BDC were used as precursors.^[101] The two reactants were placed into the glass crucibles inside the ALD reactor during the deposition process, and the sublimation temperatures were set to 190°C, 220°C for ZnAc₂ and 1,4-BDC, respectively. The MOF-5 film prepared by this method was deposited on a silicon substrate with trenches and had good conformality. The results show that the trench coverage of the entire structure is very good, and the trenches could even be completely filled. The film thickness remained constant even on high stress areas, including edges. And in 2016, Karppinen group prepared Ca-TP MOF films on Si(100) substrates using ALD (**Figure 8c**).^[102] Building on their previous study, they

expanded the temperature range of MOF film deposition (190-420°C). And the sublimation temperature was set to 190°C, 180°C for Ca(THD)₂ and 1,4-BDC, respectively. The MOF films grown by ALD had good mechanical properties and could be regenerated at a relatively low temperature.

3. Conductive Behavior in MOF Films

Metal organic framework (MOF) films are prepared via the coordination and assembly of the metal ions and organic ligands. Due to the insulating properties of organic ligands, the participation of the metal ions and the coordination bonds formed between the d-orbitals of metal ions and organic ligands, electrons cannot be effectively delocalized across the framework, which limits its application among electronic devices. Therefore, the design and preparation of the conductive MOF films have brought about widespread attention over the years. The currently reported conductive MOF films can be divided into two types: MOF films with intrinsic conductivity and MOF films with extrinsic conductivity.

3.1. Intrinsic Conductive MOFs Films

Intrinsic conductivity is derived from the inherent conductivity of metal ions or organic ligands that self-assemble into organic frameworks or coordination polymers. In this case, the design of the ligand structure and the coordination interaction between metal ion and organic ligand determine the conduction mechanism. A specific ligand is selected that will cooperate with the corresponding metal ions to generate a charge transport path, thereby obtaining a conductive MOF film. In some cases, this two-dimensional structure provides good charge delocalization, which leads to MOFs film with good conductivity.^[36]

Using organic ligand of 1,3,5-triaminobenzene-2,4,6-trithiol, Nishihara *et al.* grew multilayer and monolayers of NiAT MOF films on HMDS/Si(111) substrates by liquid-liquid interface and gas-liquid interface methods, respectively.^[103] Thickness of the monolayer can be controlled to 0.6 nm. As an electrochemical catalyst, bis(aminothiolato)nickel (NiAT) can be converted into bis(iminothiolato)nickel (NiIT) nanosheets reversibly through a proton

coupled redox reaction, leading to a sharp increase of conductivity from 3×10^{-6} to 1×10^{-1} S cm^{-1} . The change is mainly due to a clear discrepancy of band structure between NiAT and NiIT, in which NiAT shows high and persistent catalytic activity. And Zhu *et al.* also prepared two-dimensional layered Cu-BHT films with high crystallinity by the reaction of copper nitrate (II) with BHT (BHT=benzenhexathiol) at the dichloromethane/water interface(**Figure 9a**).^[62] The four probe measurements display that the conductivity of the film can achieve 1580 S cm^{-1} at room temperature, which is the highest conductivity among conductive MOFs reported thus far. It also exhibits bipolar charge transport phenomenon and great electron-to-hole mobility ($99 \text{ cm}^2 \text{ v}^{-1} \text{ s}^{-1}$ of holes and $116 \text{ cm}^2 \text{ v}^{-1} \text{ s}^{-1}$ of electrons) under field effect modulation. In addition, it shows high transmittance in the visible region, which illustrates its potential as a transparent electrode. Dincă *et al.* also used the organic ligand 2,3,6,7,10,11-hexaminitriphenylenesemiquinonate (HITP) to prepare a well-grown two-dimensional $\text{Ni}_3(\text{HITP})_2$ MOF film with the macroporous surface on a quartz substrate(a semiconducting metal-organic graphene analogue).^[104] The electrical conductivity of this film at room temperature, obtained from Van-der-Pauw measurements, was up to 40 S cm^{-1} (**Figure 9b**). With increasing temperature the electrical conductivity increased linearly and reversibly. Metals can very effectively mediate two-dimensional conjugate pathways among the electroactive organic molecules, resulting in new materials with great electrical properties.

Apart from the active ligands, the metal ions also play a great role for the conductivity of MOF films. Su *et al.* synthesized Ag_3BHT_2 and Au_3BHT_2 films with high conductivity based on the same ligand, through the liquid-liquid interface method.^[105] In this study, they used a one-step synthesis method to prepare the organic ligand BHT (**Figure 9c**). Because of its strong reactivity with metal ions, the organic ligand BHT directly interacts with the Ag or Au ions to form a MOF film. The film synthesized at the liquid-liquid interface is then transferred onto the substrate. It is worth noting that the concentration of metal ions and ligands must be strictly controlled to avoid excessively high concentrations that make the film on the interface

too thick and cause collapse. The prepared films all show high conductivity, but the conductivity of the Ag_3BHT_2 film is highest among them. This is mainly due to strong π -d conjugation between the silver ions and sulfide ions. In addition, the ordered crystal structure of Ag_3BHT_2 has a high-mode π - π superposition effect leading to high charge transport in the interlayer direction. In addition, Sun *et al.* obtained a $\text{Fe}_2(\text{DSBDC})$ MOF with the best coordination and highest conductivity by changing the metal ions and the functional group of ligand in the MOF-74 (Fe, Mn). Although the metal ions is in the same oxidation state, the increased conductivity can be attributed to the loosely bound Fe^{2+} spintronics, which highlights the advantage of Fe in the synthesis of conductive MOF materials.^[106] In general, the diversified designs of ideal metal ions and organic ligands will continuously optimize and promote the development of conductive MOF films in the fields of electronics and electrochemistry.

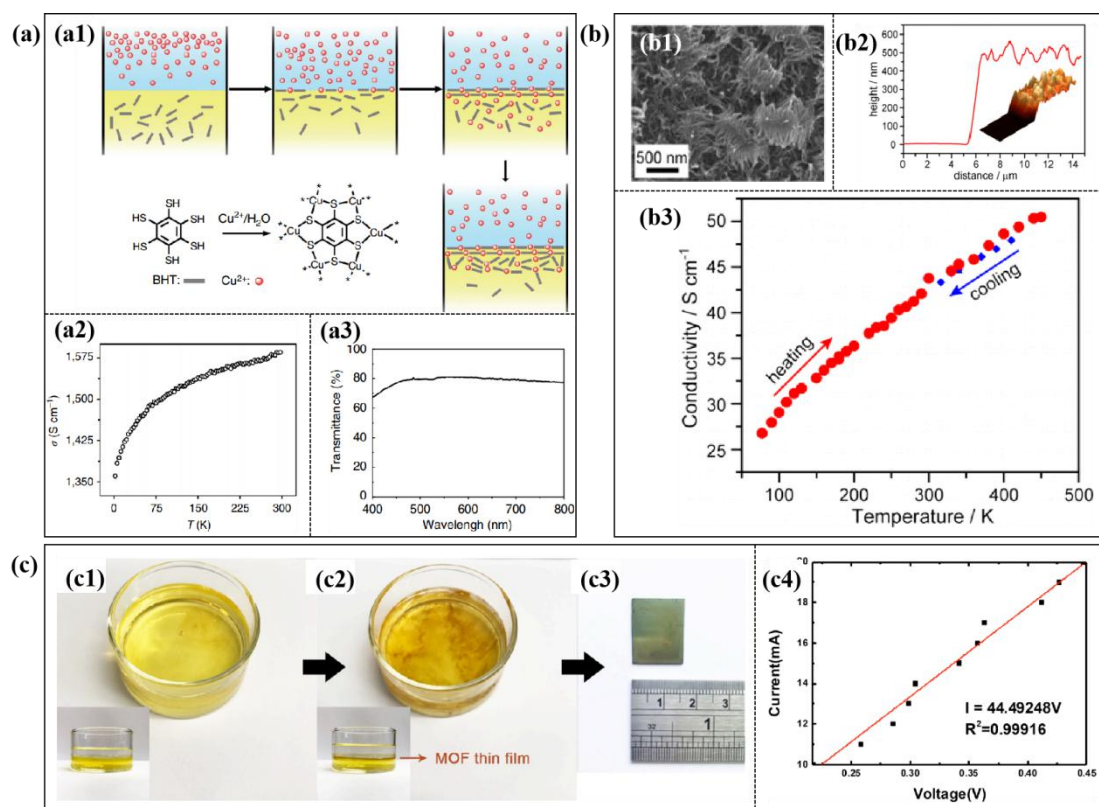


Figure 9. a1) Synthesis route of a Cu-BHT film. a2) The conductivity of the Cu-BHT film with thickness of 150 nm varies from 2 to 300 K. a3) Optical transmittance of a Cu-BHT film. The average transmittance is estimated to be 78.6%. Reproduced with permission.^[62] Copyright 2016, Nature. b1) SEM micrograph of a $\text{Ni}_3(\text{HITP})_2$ film. b2) AFM thickness distribution map and 3D AFM images of the $\text{Ni}_3(\text{HITP})_2$ film. b3) Approximately 500 nm

thick films are subjected to the van-der-Pauw conductivity measurements under variable temperatures. Reproduced with permission.^[104] Copyright 2014, American Chemical Society. c1) The state of initial reaction. c2) The process of forming a thin film. c3) Transfer the film to the substrate. c4) The I-V curve of Ag₃BHT₂ film is measured by four-probe method. Reproduced with permission.^[105] Copyright 2018, American Chemical Society.

3.2. Extrinsicly Conductive MOFs Films

3.2.1. Introduction of Redox Active Molecules

Introducing conductive guest molecules (such as dopants) into MOFs films is another effective strategy for improving their conductivity. Different types of dopants include redox active molecules, conductive polymers, and cations.

TCNQ

Redox active molecules with high electron affinity, such as TCNQ (7,7,8,8-tetracyanodimethane), can be introduced into the MOF channels, and can coordinate to the metal to form a π - π bonded charge transfer complex to obtain conductive pathways in MOFs.^[107]

Loh *et al.* adopted this method and introduced TCNQ into a MOF film, thereby demonstrating the increased conductivity of the MOF.^[108] They produced a 2D [Cu(TPyP)Cu₂(O₂CCH₃)₄] MOF film at the chloroform-water interface using interfacial synthesis, and then immersed the obtained film into a saturated dichloromethane-methanol solution of TCNQ, successfully introducing TCNQ into the Cu-MOF film. The conductivity of the initial film was very low ($\sim 10^{-7}$ S m⁻¹). After doping with TCNQ, its room temperature conductivity increased to 10⁻⁴ S m⁻¹. This result can be attributed to the formation of a charge transfer complex between the 2D Cu MOF and the TCNQ.

Talin *et al.* also proved that TCNQ enhances the conductivity of MOF films.^[109] They prepared a Cu₃(BTC)₂ film on a Si wafer, covered with SiO₂, and then transferred it to a saturated TCNQ solution, introducing TCNQ guest molecules into the nanopores of the MOF (**Figure 10a**). The conductivity of the doped MOF film increased by 6 orders of magnitude, up to 7 S m⁻¹. This increase in conductivity is mainly due to the TCNQ guest molecule

coordinating to the dual-core copper paddle wheel in the MOF frame, resulting in strong electronic coupling between the dimeric copper subunits. Therefore, the introduction of TCNQ guest molecules establishes a pathway for electron transfer.

In recent years, many researchers have introduced guest molecules into MOF films to improve their conductivity. In 2016, Deep *et al.* prepared $\text{Cu}_3(\text{BTC})_2$ films on custom-made gold wire screen printed electrodes (SPEs) by continuous impregnation.^[110] The TCNQ- $\text{Cu}_3(\text{BTC})_2$ thin films were prepared by immersing the films in a CH_2Cl_2 solution of saturated TCNQ for 48 h. The conductivity of the doped film underwent a dramatic change, increasing by nine orders of magnitude to $10^{-3} \text{ S cm}^{-1}$. Because TCNQ is a strong acceptor, TCNQ can directly coordinate to metal ions, forming charge transfer complexes with strong bonds in TCNQ- $\text{Cu}_3(\text{BTC})_2$, leading to good solid-state conductivity.

Recently, Thurmer *et al.* also introduced TCNQ into a MOF film to improve its conductivity.^[111] In this study, liquid phase epitaxy was used to deposit Cu_3BTC_2 films of different thicknesses on polycrystalline indium tin oxide (ITO) substrates, which were then immersed into a saturated solution of TCNQ in methanol (**Figure 10b**). The results showed that the Cu_3BTC_2 film reacts with the TCNQ methanol solution to form a dense $\text{Cu}(\text{TCNQ})$ coordination polymer film. This chemical transformation is accompanied by a sharp change in conductivity, from $<10^{-11} \text{ S cm}^{-1}$ of Cu_3BTC_2 film before doping to $10^{-1} \text{ S cm}^{-1}$ for the doped film, an increase of 10 orders of magnitude.

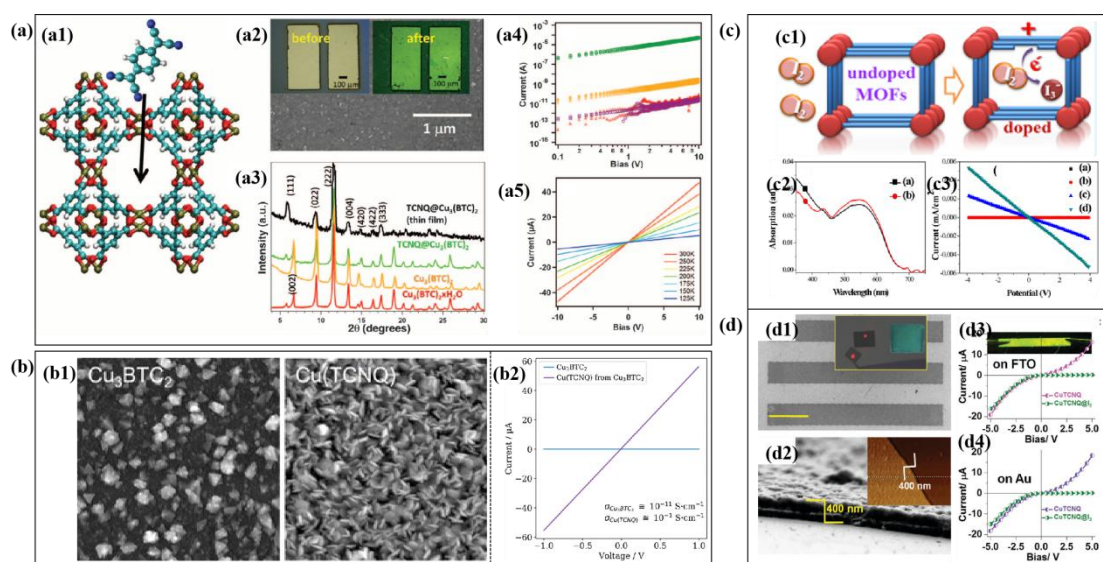


Figure 10. a1) Schematic diagram of the process of TCNQ molecules entering $\text{Cu}_3(\text{BTC})_2$ MOF. a2) SEM image of a $\text{Cu}_3(\text{BTC})_2$ MOF-covered device. The inset is an optical image of the device before and after the TCNQ treatment. a3) XRD data of powder samples and grazing incidence XRD of film. a4) I-V curve before (red) and after treatment with TCNQ (green), F_4 -TCNQ (gold) and H_4 -TCNQ (purple). a5) Temperature dependence of the I-V curve. Reproduced with permission.^[109] Copyright 2014, Science. (b1) SEM images of a $\text{Cu}_3(\text{BTC})_2$ film before and after doping with TCNQ. b2) Change of conductivity of a $\text{Cu}_3(\text{BTC})_2$ film before and after TCNQ doping. Reproduced with permission.^[111] Copyright 2018, American Chemical Society. c1) Schematic diagram of the I_2 doping process of MOFs. c2) UV-visible absorption spectrum of a $\text{Co}_3(\text{NDC})_3$ MOF film on the amine functionalized glass slides via LBL technology: (a) as prepared MOF film (b) Iodine-doped MOF film. c3) I-V curve of a $\text{Co}_3(\text{NDC})_3$ MOF film: undoped doctor-bladed film (a), undoped LBL film (b), iodine-doping doctor-bladed film (c) and Iodine-doped LBL film. Reproduced with permission.^[112] Copyright 2015, American Chemical Society. d1) Cu-TCNQ SURMOF patterned thin film device grown on an FTO substrate. d2) Cross-sectional FESEM image exhibiting the thickness of a patterned Cu-TCNQ SURMOF thin film. d3) I-V curves of the Cu-TCNQ SURMOF grown on a FTO board before and after I_2 vapor treatment. d4) I-V curves of a Cu-TCNQ SURMOF grown on Au before and after treatment of I_2 vapor. Reproduced with permission.^[114] Copyright 2016, Wiley-VCH.

I_2

Doping the nanochannels of MOFs with I_2 by immersing the MOF into a I_2 solution or exposing it to I_2 vapor facilitates the interactions between organic ligands, thereby resulting in the generation of charge carriers (holes) in the framework when the $n \rightarrow \sigma^*$ molecular transition induces charge transfer.^[112] Many MOFs show good conductivity after I_2 is infiltrated into their nanopores. Han *et al.* used this method to improve the conductivity of MOFs by introducing I_2 into MOF films (**Figure 10c**). In the doping process, $\text{Co}_3(\text{NDC})_3$ thin films were synthesized via LBL and doctor blade (DB) methods, respectively, and then the

MOF films were immersed into an acetonitrile solution containing I_2 at 50°C . The results show that the undoped films are insulators, while the films doped with I_2 are p-type semiconductors. This change can be mainly ascribed to the formation of the charge transfer complexes, which introduces the hole doping into the MOF films.

Shrestha *et al.* prepared a Cu_3BTC_2 film by LBL deposition, and then immersed it into an acetonitrile solution of I_2 .^[113] As a result, the film changed from an insulator to a conductor ($2.43 \times 10^{-6} \text{ S cm}^{-1}$). This is mainly due to the conductive pathway formed by the interaction between host MOF and guest molecules. The doped modified film was used as the absorption layer of a solar cell, with an energy conversion efficiency of 0.26%, and it successfully reduced the charge transfer resistance at the $\text{TiO}_2/\text{MOF}/\text{electrolyte}$ interface.

Recently, the I_2 doping process has also influenced the conductivity of other MOF films. Ballav *et al.* applied liquid phase epitaxy to directionally grow a uniform Cu-TCNQ film on a MUDA/Au SAM substrate and found that it shows very high hydrophobicity.^[114] A Cu-TCNQ thin film lithography device, prepared using electron beam lithography, showed non-ohmic semiconductor properties, and the conductivity significantly improved after the film was exposed to I_2 vapor (**Figure 10d**). The high hydrophobicity was retained even after I_2 doping. The improvement of the film due to I_2 can be mainly attributed to the structure and electronic recombination in the SURMOF.

3.2.2. Introduction of a Conductive Polymer

Polymerizable monomers can be inserted into the pores of a MOF as guest molecules and then polymerized in the pores. Low-molecular-weight monomers have higher mobility than their corresponding polymers, and can be introduced into the MOF nanochannels in large quantities and undergo irreversible polymerization. The polymer chains formed in the nanochannels are kinetically captured and cannot be released without decomposing the backbone of polymer chain. Thus far, in-situ polymerization is the most commonly used technique for preparing polymer@MOF composites. In addition, polymerization in a confined space can yield

polymers with controllable structures, which is essential for adjusting and enhancing the function of hybrid materials.^[115,116]

In 2018, Lu *et al.* introduced aniline (An) into Zr-MOFs using this strategy and formed a Zr-MOF/PAn/PSS composite film by APS (ammonium persulfate)-catalyzed oxidative polymerization inside the pores.^[117] During the doping process, the polystyrene sulfonic acid was used as the dopant, and polyaniline (PAn) chains interpenetrated into the whole Zr-MOFs, enhancing the crystallinity of PAn and increasing the conductivity of the MOF film (**Figure 11a**). The thermoelectric properties of the material can be adjusted by controlling the amount of the Zr-MOF. When 20 wt% Zr-MOF was used to prepare the film, the conductivity and power factor of the composites film reached unprecedented maximum values of 2.10 S m^{-1} and $664 \mu\text{W (mK}^2)^{-1}$, respectively. In addition, compared with a PAn/PSS film, the electrical conductivity and power factor of the composite film also prominently improved.

Similarly, Zhang *et al.* demonstrated the importance of introducing conductive polymers into MOF films for improving their conductivity.^[118] They used a solvothermal method to prepare a UiO-66 MOF film on cotton cloth (CT), and then introduced pyrrole (Py) molecules into the MOF channel, finally obtained a PPy@UiO-66@CT composite material by the catalysis of FeCl₃-methyl orange complex (**Figure 11b**). Because of its excellent conductivity and one-dimensional structure, PPy nanotubes can be used as a conductive connector between UiO-66 particles. And the measured conductivity was 14.29 S cm^{-1} , this strategy of constructing conductive MOFs can enrich the types and application range of conductive MOFs.

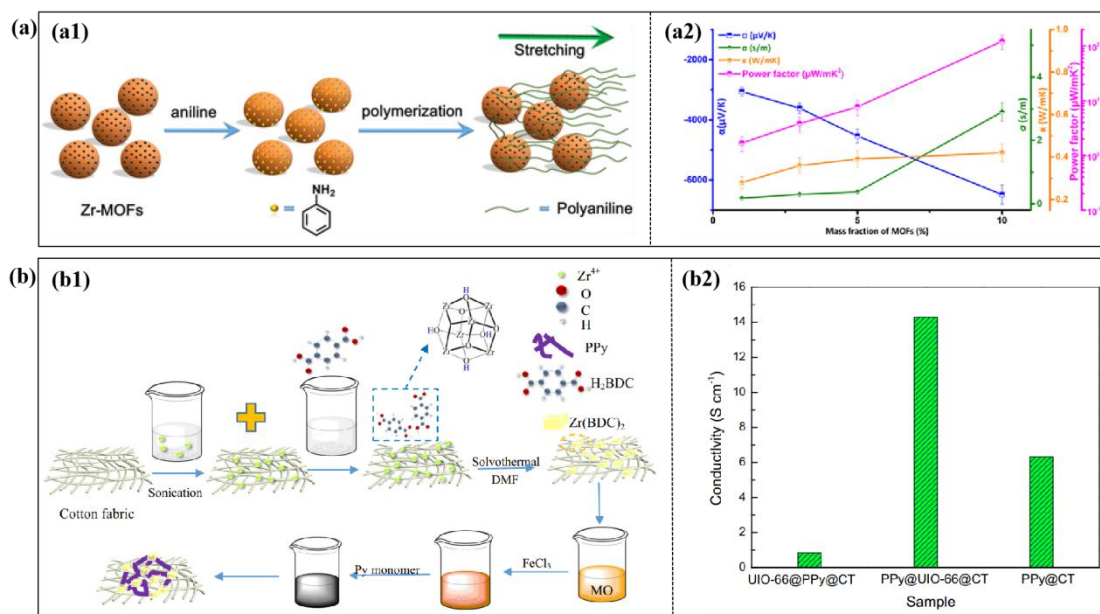


Figure 11. a1) Schematic of the formation process of composite Zr-MOF/PAn. a2) Thermoelectric properties (Seebeck coefficient ($|\alpha|$), thermal conductivity (κ), electrical conductivity (σ) and power factor) as a function of the load of the Zr-MOF in the ZB-A/PAn/PSS film. Reproduced with permission.^[117] Copyright 2018, American Chemical Society. b1) Schematic of the synthesis of the PPy@UiO-66@CT. b2) Conductivity of the PPy@CT, the UiO-66@PPy@CT and the PPy@UiO-66@CT. Reproduced with permission.^[118] Copyright 2019, Springer Nature.

3.2.3. Introduction of Cations

Cations can be easily assembled into the pores of MOFs, which can enhance the conductivity while maintaining the porosity of the framework. In MOFs, most ligands lack redox activity, and the large space distance between ligands hinders the charge transfer through space. Guest molecules containing π moieties and being able to interact with ligands can be used to create charge transport paths in MOFs. Saha *et al* reported a novel blue electroactive BMOF constructed by N,N'-bis(4-pyridyl)-2,6-dipyrrolydyl naphthalenediimide(BDPNDI) pillars and 1,2,4,5-tetrakis-(4-carboxyphenyl)benzene(TCPB) (**Figure 12**).^[119] Then, the synthesized BMOF films were assembled on ZnO-FTO-glass substrates under solvothermal conditions, and then were immersed in the cationic methyl viologen (MV^{2+}) solution, and finally a doped modified BMOF thin film was prepared. The electrical conductivity of the BMOF film before and after doping processes measured by the four-probe method are $6 \times 10^{-5} \text{ S m}^{-1}$ and $2.3 \times 10^{-3} \text{ S m}^{-1}$, respectively. It is illustrated for the first time that the conductivity of BMOF films can

be adjusted by introducing π -acid guest molecules, which are inserted between the BDPNDI pillars, thereby promoting electron delocalization through π -stacks.^[120,121]

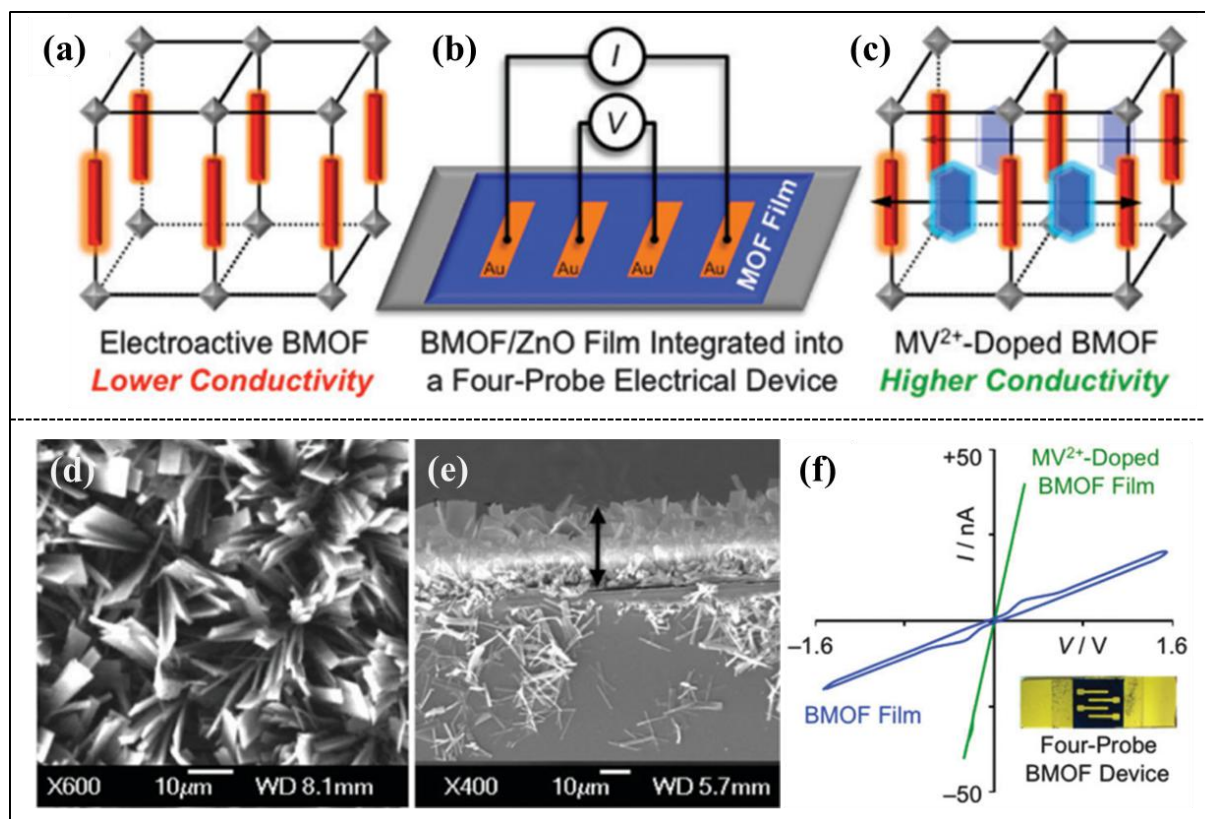


Figure 12. a) An electroactive MOF made of redoxactive ligands. b) Four-probe electronic device composed of electroactive MOF film grown on ZnO-coated surface. c) The BMOF film doped with MV^{2+} has higher conductivity. d-e) SEM images of a BMOF film, cross-sectional SEM image of BMOF/ZnO film. f) I-V relationship diagram of BMOF/ZnO-glass equipment before and after doping with MV^{2+} . Reproduced with permission.^[119] Copyright 2015, Royal Society of Chemistry.

4. Applications

Conductive MOFs are a kind of multifunctional hybrid material, combining somewhat the properties of both inorganic and organic materials, and have the advantages of rich and diverse structures, designable frame and pore structures, large surface areas, and good electrical conductivity. This leads to their wide application potential in many fields, including in chemical resistance gas sensors, supercapacitors, electrocatalysts and other electrochemical fields.

4.1. Electrochemical Sensing

Gas detection plays a very important role in environmental protection,^[122] personalized medicine,^[123] and the chemical industry.^[124] Chemical resistance sensors are perfect devices for portable gas detection ascribing to their high selectivity and sensitivity. Conductive MOF materials are very attractive materials for chemical resistance sensing applications ascribing to their ultra-high specific surface area and adjustable pore structure. Thus far, most conductive MOF devices are made of powders and thick films, which seriously affects the quality and electronic transmission in these electronic devices. In order to enhance the performance of these electronic devices, it is necessary to manufacture the high-quality two-dimensional conductive MOF films with a controllable thickness on the nanometer scale.

Xu *et al.* prepared a two-dimensional conductive $\text{Cu}_3(\text{HHTP})_2$ film with a smooth surface, a controllable thickness, and good orientation using liquid phase epitaxy.^[43] The room temperature conductivity of the MOF film (thickness, 20 nm) was 0.02 S cm^{-1} . This good conductivity results from the strong charge delocalization between the copper ion and the ligand. The conductive $\text{Cu}_3(\text{HHTP})_2$ film had excellent room temperature sensing performance (**Figure 13a**), could selectively detect NH_3 against 10 typical interfering gases, and exhibited the great sensing capacity for 10 ppm NH_3 (response = 45%). The limit of detection is as low as 0.5 ppm, because the electron transport in the two-dimensional conductive MOF film is very sensitive to NH_3 adsorption, and the film had long-term stability and repeatability for sensing.

Mirica *et al.* applied the self-assembly of metal ions (Ni) and organic ligands (HHTP or HITP) to grow two-dimensional conductive Ni_3HHTP_2 and Ni_3HITP_2 MOF films on a fiber fabric substrate, thus rapidly preparing multi-functional electronic textiles.^[44] Since the two-dimensional conductive MOFs were firmly bound to the fabric matrix, the synthesized composite fabric exhibited good electrical conductivity, mechanical stability and high flexibility (**Figure 13b**). The composite fabrics showed high responses to 80 ppm NO ($\Delta G/G_0=81\%$ of Ni_3HITP_2) and H_2S ($\Delta G/G_0=98\%$ of Ni_3HHTP_2). In addition, the sensor

maintained its performance at a humidity of 18% (5000 ppm), and could be fully recycled and cleaned. The theoretical detection limits of the sensor are 0.16 ppm, 0.23 ppm for NO and H₂S, respectively.

Due to the ongoing study of MOF materials in recent years, the shortcomings of using a single MOF layer with its functional limitations have made the design and preparation of heterostructure multilayer MOF films a focus of research. Xu *et al.* used a Van-der-Waals integration method, that overcomes the limitation of lattice matching, to deposit a molecularly sieved Cu-TCPP layer on a Cu-HHTP layer to obtain a MOF-on-MOF film with controllable thickness and high orientation (**Figure 13c**).^[125] The Cu-TCPP-on-Cu-HHTP film exhibited splendid selectivity, long-term stability and the highest response to benzene reported at room temperature, and had a reverse selectivity for benzene and NH₃.

Although two-dimensional conductive MOFs exhibit exciting performance and good stability, studies of these MOFs mainly concentrate on systems with redox active ligands and a single metal or bimetal node. However, the two-dimensional conductive MOF films with double ligands have not been reported. Wu *et al.* used liquid phase epitaxy to prepare a nano-scale, dual-ligand conductive MOF film with a smooth surface on a -OH functionalized substrate.^[126] After 10 cycles of alternate exposure in a mixed solution of metal ions and two organic ligands, HHTP-doped Cu-HHTP-10C nanofilms with different doping ratios were prepared. The results show that the selectivity of HHTP-doped Cu-HHTP-10C nanofilms for benzene over NH₃ ($S=R_{\text{benzene}}/R_{\text{NH}_3}$) gradually increases with increasing HHTP ligand doping in the Cu-HHTP framework. Because HHTP doping produces defects, the selectivity for benzene over NH₃ increases by more than 220%. In addition, appropriate HHTP doping also improves the sensor response and recovery performance.

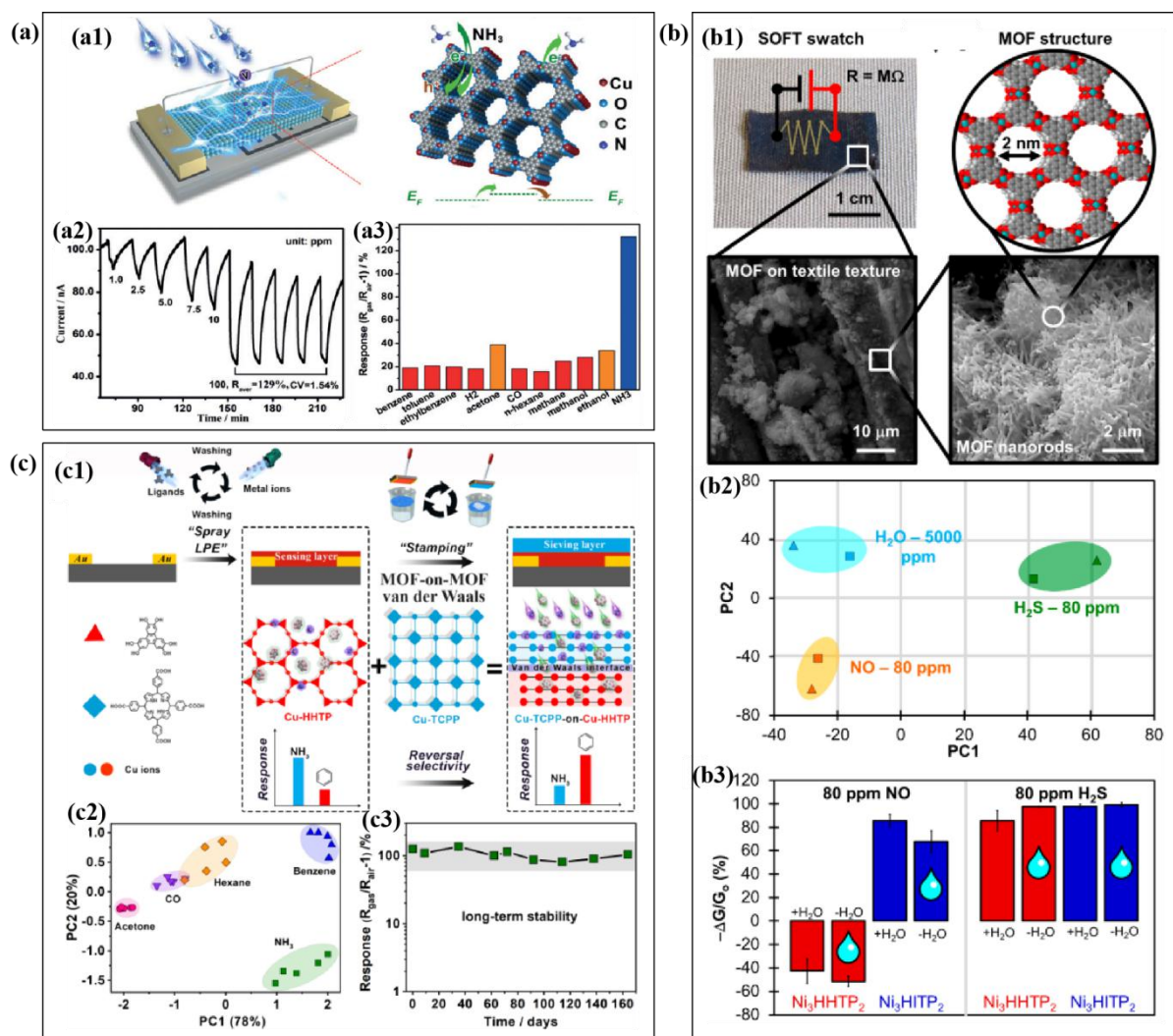


Figure 13. Application of a conductive MOF film in electrochemical sensing. a1) The gas sensor of conductive $\text{Cu}_3(\text{HHTP})_2\text{-10C}$ film and the possible gas-sensing mechanism. a2) The response–recovery curves of NH_3 for $\text{Cu}_3(\text{HHTP})_2\text{-10C}$ film under different concentrations. a3) Column chart of the responses of $\text{Cu}_3(\text{HHTP})_2\text{-10C}$ to different reducing gases. Reproduced with permission.^[43] Copyright 2017, Wiley-VCH. b1) Conductive MOF (Ni_3HHTP_2 or Ni_3HITP_2) nanowires coated textile texture as the gas sensor and the images of its microstructures. b2) Comparison of the ability of Ni_3HHTP_2 and Ni_3HITP_2 flexible sensors to distinguish NO, H_2S and H_2O . b3) Gas sensing capacities of Ni-CAT and Ni_3HITP_2 based devices to 80 ppm NO and H_2S under dry and humidified environments (5000 ppm H_2O). Reproduced with permission.^[44] Copyright 2017, American Chemical Society. c1) Schematic illustration of the synthesis process of MOF-on-MOF thin films by vdW integration and their application as the sensing materials for highly selective benzene. c2) PCA for MOF-on-MOF sensor array's response to five representative biomarkers. c3) Long-term stability of Cu-TCPP-10C-on-Cu-HHTP-20C toward 100 ppm benzene gas. Reproduced with permission.^[125] Copyright 2019, Wiley-VCH.

4.2. Supercapacitors

For satisfying the increasing demand for sustainable and renewable energy, there is an urgent requirement to develop high-efficiency energy conversion and storage technologies.

Supercapacitors have become a promising energy storage device due to their high power density, long cycle life, operational safety and reliability.^[127] The active electrode material is the key part of the supercapacitor, and carbon-based materials are the main electrode materials that are being studied at present.^[128] However, there is a clear opportunity for the development of new and improved electrode materials. Metal organic frameworks (MOFs) are materials with much larger surface area than activated carbon, which will challenge the dominance of carbon electrodes in EDLCs. Conductive MOFs can be directly used as the electrode materials for the supercapacitors because of their many pseudocapacitance redox sites and high surface area. The area capacitance of MOF based supercapacitors exceeds that of most carbon based materials, and the capacity retention rate is still more than 90% after 10000 cycles.^[17]

Zhao *et al.* first applied a surfactant-assisted synthesis method to prepare wrinkled two-dimensional ultrathin Cu-TCPP nanosheets.^[45] By combining the electrophoretic deposition and the electrochemical polymerization processes, the obtained Cu-TCPP nanosheets are combined with conductive polypyrrole (PPy), and then the nanosheets are further layered to prepare a flexible and independent Cu-TCPP/PPy film (**Figure 14a**). The synergistic effect of the Cu-TCPP and PPy shortens the electrolyte ion transport pathway, provides a macroporous channel for the fast ion/electron transport and a three-dimensional conductive network for the fast electron transport. Cu-TCPP/PPy has higher supercapacitance performance compared to a single nanosheet. The Cu-TCPP/PPy film electrode shows a capacitance of 340.6 mF cm^{-2} at 1 mA cm^{-2} , which is 45% higher than the original PPy film (224.6 mF cm^{-2}) at the corresponding current density. In addition, they prepared the Cu-TCPP/PPy-based symmetric supercapacitor that has a maximum energy density of $2.27 \text{ } \mu\text{W h cm}^{-2}$ at the highest power density of $50 \text{ } \mu\text{W cm}^{-2}$.

It is well known that the selection of the ligand plays an important role in the design of conductive MOFs. When using larger ligands to construct 2D and 3D MOFs, the low inherent

density of the framework limits the theoretical density of redox active sites and the achievable weight and volume capacitance of the MOF. Therefore, choosing a smaller ligand not only yields a high density framework, but also improves the capacitance. Bao *et al.* reported a two-dimensional conductive Ni-HAB and Cu-HAB MOF based on the organic ligand of HAB.^[129] The synthesized MOF has an ultra-high volume capacitance of 760 F cm^{-3} and a high area capacitance of more than 20 F cm^{-2} (**Figure 14b**). The MOF electrode shows good cycling stability, and 90% capacity preservation even after 12,000 cycles, and exhibits fantastic chemical stability in the acidic and basic aqueous solutions.

At present, flexible transparent supercapacitors are considered to be a key energy storage element for powering smart portable electronic devices. However, preparing flexible transparent capacitor electrodes with high rate performance still faces huge challenges. Huang *et al.* fabricated a conductive Ni_3HITP_2 film on an ITO/PET substrate using gas-liquid interfacial synthesis and used it as the capacitor electrode for a flexible transparent supercapacitor.^[46] The Ni_3HITP_2 electrode has an excellent photoelectric performance of 78.4%(T, optical transmittance), surface capacitance performance C_A of 1.63 mF cm^{-2} , and a rate performance of 5000 mV s^{-1} . As shown in **Figure 14c**, as the optical transmittance (T) decreasing, the sheet resistance (R_s) increases with a longer reaction time. The corresponding symmetric/asymmetric all-solid supercapacitors have excellent surface capacitance performance and extraordinary rate capabilities.

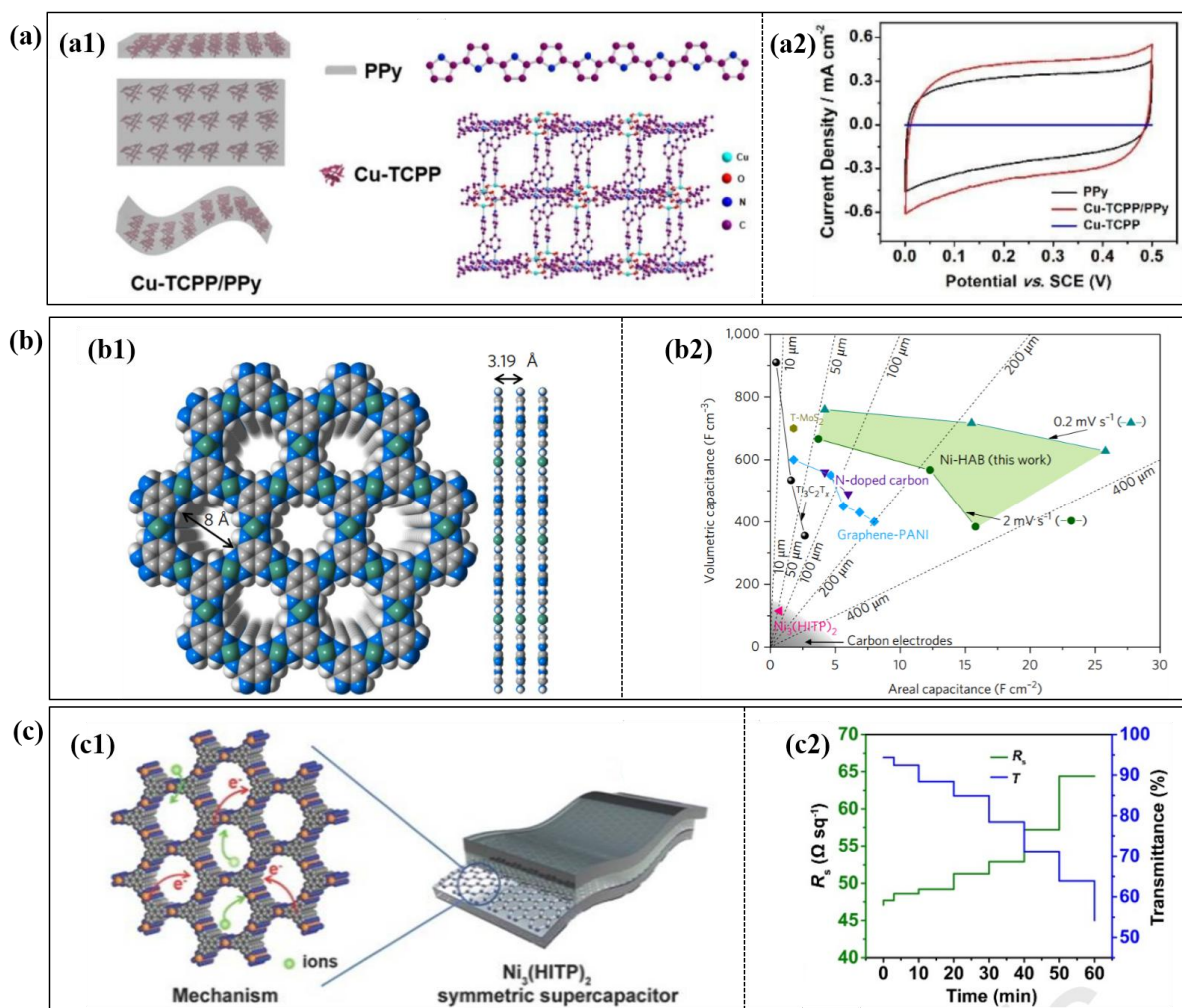


Figure 14. Application of conductive MOF films in supercapacitors. a) Cu-TCPP/PPy conductive MOF film. a1) Schematic diagram of a Cu-TCPP/PPy film and crystal structure of PPy and Cu-TCPP. a2) CV curves of the Cu-TCPP/PPy, PPy, and Cu-TCPP films at a scan rate of 1 mV s^{-1} . Reproduced with permission.^[45] Copyright 2019, Royal Society of Chemistry. b) 2D conductive Ni-HAB and Cu-HAB MOFs. b1) Cu-HAB spatial structure model. b2) Comparison of the surface and bulk capacitances of a Ni-HAB electrode and other materials. Reproduced with permission.^[129] Copyright 2018, Nature. c) A conductive $\text{Ni}_3(\text{HITP})_2$ film. c1) $\text{Ni}_3(\text{HITP})_2$ film as electrode material in a symmetric capacitor and its conduction mechanism. c2) The R_s and T of a $\text{Ni}_3(\text{HITP})_2/\text{ITO}/\text{PET}$ electrode under different preparation time. Reproduced with permission.^[46] Copyright 2020, Elsevier.

4.3. Electrocatalysis

For the past few years, conductive MOFs have been widely used as electrocatalysts ascribing to their ultra-high specific surface area, adjustable porous structure, and inherent electronic properties, including in the hydrogen evolution reaction (HER), oxygen evolution reaction (OER) and oxygen reduction reaction (ORR).

The availability of highly efficient HER catalysts is critical for solar energy technologies with the purpose of reducing future carbon emissions. The HER forms hydrogen by catalyzing the combination of protons and electrons in solution. Hupp *et al.* reported an efficient and low-cost MOF film based HER electrocatalyst.^[130] They deposited a NU-1000 MOF film on a glass-supported FTO electrode using a solvothermal method, and then used electrodeposited Ni-S onto the FTO_NU-1000 film to obtain NU-1000_Ni-S, a hybrid electrocatalyst that shows good hydrogen evolution activity (**Figure 15a**). Compared with pure Ni-S without the MOF, the obtained hybrid material has a significantly enhanced HER performance in HCl aqueous solution at pH=1, and the kinetic overpotential decreases by more than 200 mV at a reference current density of 10 mA cm⁻². This is mainly due to the effect of the NU-1000 MOF on the local environment of the electrocatalyst, which in turn changes the catalytic activity of the metal-sulfide electrode and significantly decreases its overpotential.

The OER, an important part of fuel cells, water splitting and rechargeable batteries, has never been successfully catalyzed by a two-dimensional conductive MOF with few layers. Zhang *et al.* synthesized a new type of π -conjugated conductive metal organic nanosheet with few layers using the LB method,^[131] which successfully catalyzed the OER reaction (**Figure 15b**). The results show that the 4-layer [Co₃(HHTP)₂]_n electrode exhibits a low onset potential, ultra-high mass activity (64.63 A mg⁻¹) and long-term stability for the OER in basic media.

At the same time, Du *et al.* developed a new type of nickel-based phthalocyanine two-dimensional conductive MOF.^[132] They prepared NiPc-MOF thin film on FTO substrates using the bottom-up method (**Figure 13c**). The thin films exhibited excellent catalytic OER activity, with a relatively low onset potential (1.48 V) and high quality activity (883.3 A g⁻¹). In addition, the OER catalysis of NiPc-MOF showed good durability.

The ORR is the electrocatalytic reduction of molecular oxygen on the electrode surface, which plays a crucial role in the energy conversion devices.^[133] At present, platinum-based precious metal catalysts are still the main electrocatalysts for the ORR.^[134] Therefore, it is urgently needed to find low cost ORR catalysts with excellent electrocatalytic activity. Conductive MOFs have gradually become new robust active electrocatalysts for the ORR. Dincă *et al.* deposited a conductive $\text{Ni}_3(\text{HITP})_2$ MOF film (thickness, ~ 120 nm) on a glassy carbon electrode using a solvothermal synthesis and applied it directly as an ORR catalyst.^[135] And the inherent high surface area and porosity of $\text{Ni}_3(\text{HITP})_2$ increased the density of $\text{Ni}_3(\text{HITP})_2$ and made it easy to obtain catalytically active sites, thereby significantly promoting the ORR activity. $\text{Ni}_3(\text{HITP})_2$ exhibited a superoxide reduction potential of 0.18 V in 0.10 M KOH and structural stability during electrochemical cycling under O_2 .

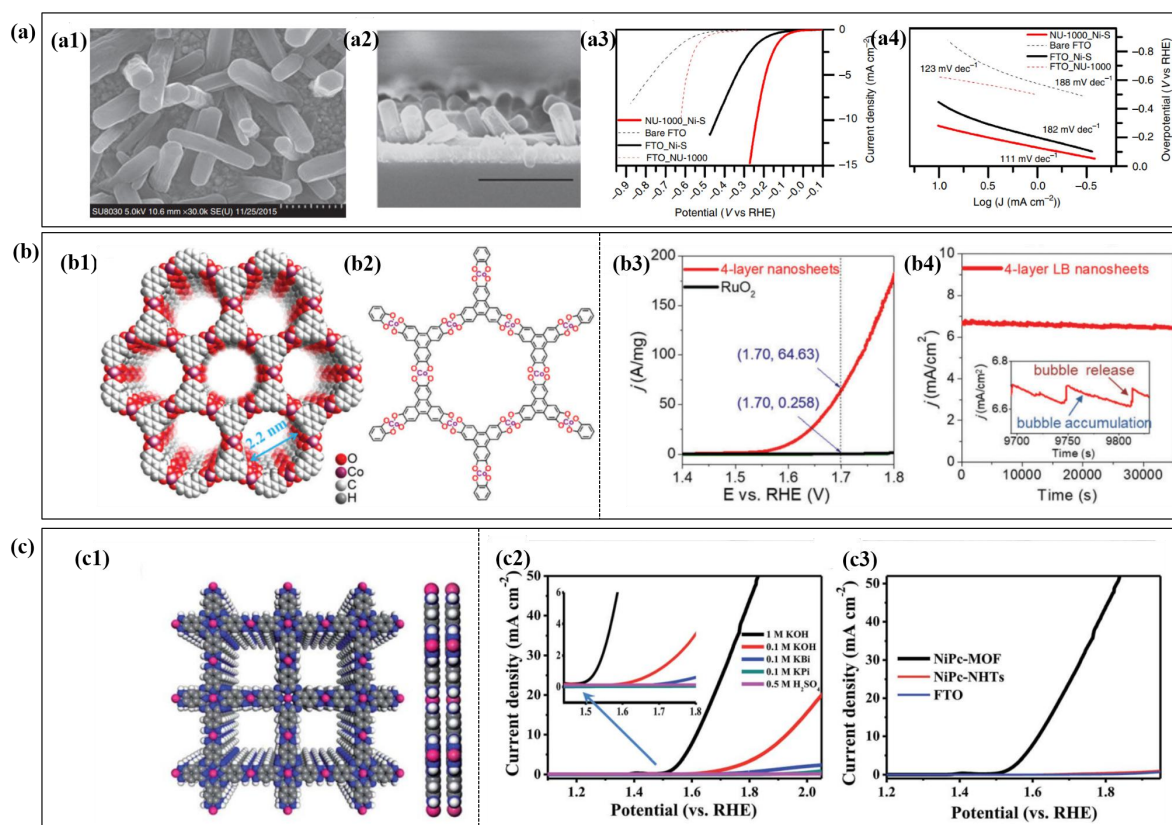


Figure 15. Application of conductive MOF films in electrocatalysis. a) NU-1000_Ni-S conductive MOF film. a1) SEM image of a NU-1000_Ni-S film. a2) SEM image of cross section of the NU-1000_Ni-S film. Comparison of electrocatalytic performance of four electrodes a3) J-V curve. a4) Tafel plot. Reproduced with permission.^[130] Copyright 2015, Nature. b) A $[\text{Co}_3(\text{HHTP})_2]_n$ conductive MOF film. b1) $[\text{Co}_3(\text{HHTP})_2]_n$ crystal structure along the channel direction. b2) The connection between HHTP molecule and Co^{2+} ion. b3) J-A/mg plot. b4) J/cm² vs Time plot. c) NiPc-MOF. c1) NiPc-MOF crystal structure. c2) J-V curve. c3) J-V curve.

LSV curve of a 4-layer $[\text{Co}_3(\text{HHTP})_2]_n$ LB nanoflake and RuO_2 in the unit weight range. b4) The variation of the current density at 1.7V with time^l. Reproduced with permission.^[131] Copyright 2018, Royal Society of Chemistry. c) A NiPc–MOF conductive film. c1) Eclipsed AA-stacking mode of NiPc-MOF. c2) The pH-dependent LSV curve of NiPc-MOF as an OER catalyst. c3) LSV curve of NiPc-MOF, NiPc-NHTs monomer and blank FTO as OER catalyst. Reproduced with permission.^[132] Copyright 2018, Royal Society of Chemistry.

4.4 Electronic Devices

4.4.1. Field Effect Transistors

The field effect transistor (FET) is a three terminal semiconductor device that plays an important role in modern electronic applications due to its high integration, mass production and adjustable electrical performance.^[136-138] However, conductive MOF materials with high crystallinity, microporous structures and low dielectric constants provide a new candidate material for the modified FET dielectric layer.^[139-141] In 2017, Zhang *et al.* First prepared the field effect transistors based on a thin film of the SURMOF HKUST-1, using liquid phase epitaxy.^[142] By controlling the number of LPE cycles used during the preparation of $\text{Cu}_3(\text{BTC})_2$, the charge mobility and threshold voltage can be effective controlled and optimized. The results illustrated that the performance of the HKUST-1/ SiO_2 -based OFET is significantly better than that of a pure SiO_2 -based OFET (**Figure 16a**). The performance enhancement of the device can be mainly ascribed to the high crystallinity, homogeneous material and the smaller interface trap density of the OFET.

In order to prepare a smooth and dense conductive MOF film and improve its quality, Xu *et al.* for the first time successfully prepared a porous FET based on a $\text{Ni}_3(\text{HITP})_2$ MOF film using gas-liquid interfacial synthesis (**Figure 16b**).^[30] The FET exhibits P-type behavior, an on-off current ratio of 2×10^3 , and excellent field-effect hole mobility of $48.6 \text{ cm}^2 \text{ V}^{-1} \text{ s}^{-1}$. The porous channels in the MOFs greatly expand the application range of FETs, leading to potential applications in the field of channel materials with large surface area and penetration abilities.

Currently, it is still challenging to prepare a large area MOF film that is undamaged after being transferred to the substrate. Duan et al. fabricated a large area NiMOF-FET with good uniformity and controllable thickness on a Si/SiO₂ substrate using an *in situ* growth strategy based on a solid-liquid interface (**Figure 16c**).^[29] The thickness and density of the MOF film can be controlled by changing the reaction time. In the field effect transistor, the Ni₃(HITP)₂ film was used as the channel material, which has a good mobility of 45.4 cm² V⁻¹ s⁻¹ and an on/off current ratio of 2.29×10³. The produced FET was used in a biosensor device for glucose detection.

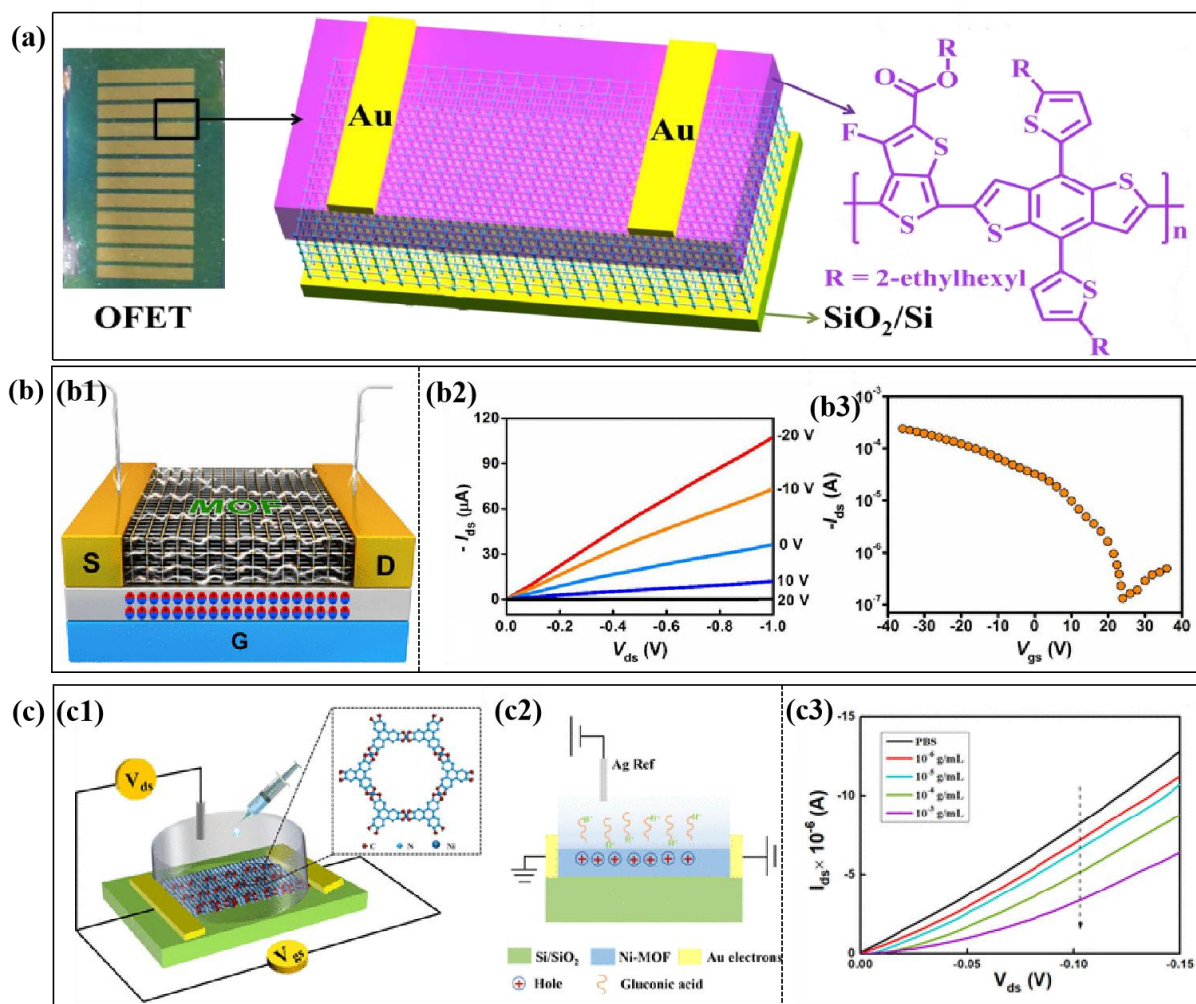


Figure 16. Application of conductive MOF film in field effect transistor. a) Schematic diagram of OFET structure after MOF HKUST-1 film modified SiO₂ dielectric layer interface and the chemical structure of the semiconductor polymer PTB7-Th. Reproduced with permission.^[142] Copyright 2017, American Chemical Society. b) MOF-based porous field effect transistor. b1) Schematic illustration of Ni₃HITP₂-based porous FETs. b2) Output curves of Ni₃HITP₂-based FETs. b3) Transfer curves of Ni₃HITP₂-based FETs. Reproduced with permission.^[30] Copyright 2016, American Chemical Society. c) Schematic diagram of

Ni-MOF-FET. c1) MOF-based liquid-gated field-effect transistor. c2) Detection of gluconic acid under negative gate voltage. c3) I_{ds} - V_{ds} graph of Ni-MOF-FET exposed to $10^{-6} \sim 10^{-3}$ g/mL gluconic acid. Reproduced with permission.^[29] Copyright 2019, American Chemical Society.

4.4.2. Organic Spin Valve

Organic spin valves (OSVs), a typical organic spin electron device, show significant potential for quantum computing and data storage.^[143] OSVs are mainly composed of two ferromagnetic (FM) electrodes with different forced fields and a nonmagnetic (NM) organic interlayer.^[144] Recently, conductive MOF films have been combined with organic spin valves to motivate the potential applications of new generation OSVs. In 2019, Chen *et al.* for the first time used layer-by-layer deposition self-assembly to prepare a highly crystalline, highly oriented conductive $\text{Cu}_3(\text{HHTP})_2$ MOF film on a $\text{La}_{0.67}\text{Sr}_{0.33}\text{MnO}_3$ (LSMO) ferromagnetic electrode with a controllable thickness (**Figure 17**).^[28] When the thickness of the $\text{Cu}_3(\text{HHTP})_2$ film was 30-100 nm, the OSVs showed a magnetoresistance (MR) effect. The MOF film was used as the non-magnetic spacer layer in the OSV. The assembled LSMO/ $\text{Cu}_3(\text{HHTP})_2$ /Co OSV had a magnetoresistance of 25% at 10 K. Although studies have shown that the exact spin-polarized transport physics is still elusive, the development of appropriate 2D π -d conjugated MOFs through appropriate chemical design is necessary for the regulation of their electronic structure and spin transport pathways.

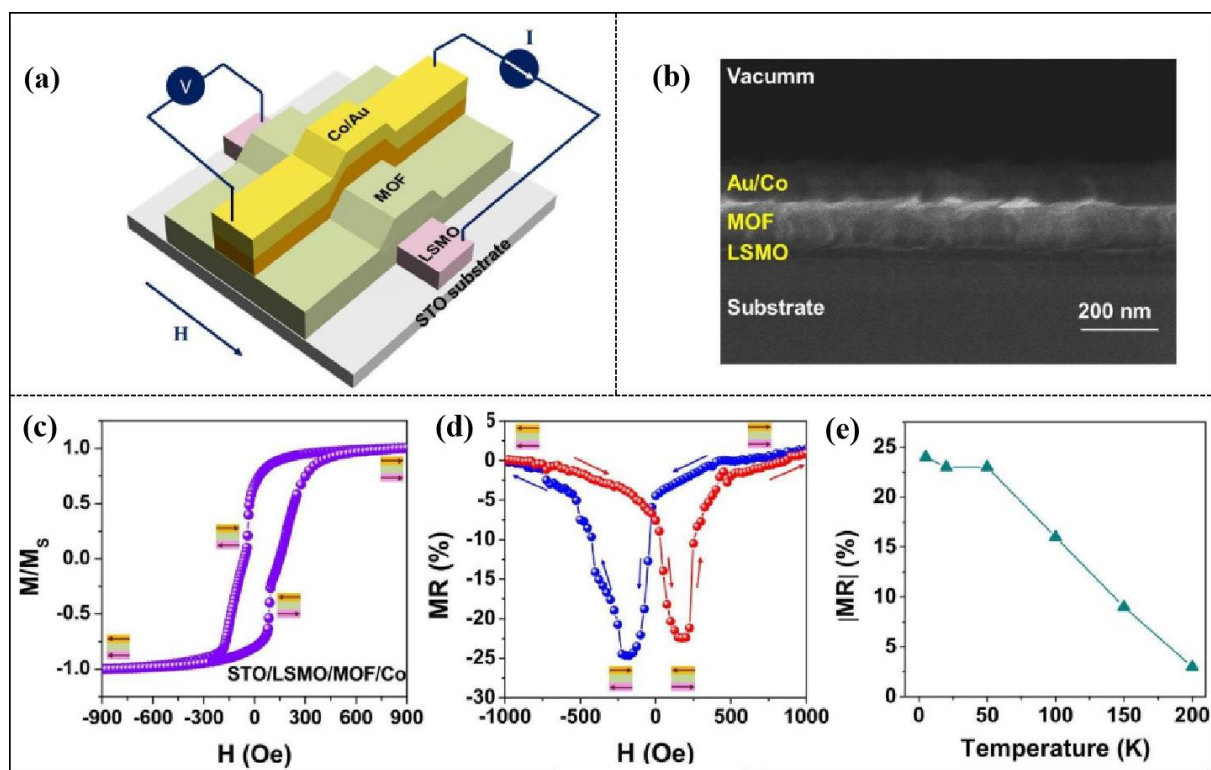


Figure 17. 2D conductive MOF-based organic spin valves. (a) Schematic diagram of vertical OSVs. (b) SEM image of vertical OSV cross section. (c) Hysteresis loop. (d) Hysteresis loop of OSVs at 10 K. (e) Temperature dependence of MR value. Reproduced with permission.^[28] Copyright 2020, Wiley-VCH.

Table 1. List of conductive MOF films with name, synthetic methods, doping strategies, conductivities, and corresponding applications.

MOFs film	Synthetic methods	Doping strategies	Conductivity (S cm ⁻¹)	Applications	Reference
NiAT	Liquid-liquid interface and gas-liquid interface	Intrinsic	1×10^{-1}	Electrocatalysis (HER)	[103]
Cu-BHT	Liquid-liquid interface	Intrinsic	1580	Transparent electrodes	[62]
Ni ₃ (HITP) ₂	Solvotherm (<i>In situ</i>)	Intrinsic	40	-	[104]
Ag ₃ BHT ₂ Au ₃ BHT ₂	Liquid-liquid interface	Intrinsic	363 1.12×10^{-4}	Sensors	[105]
[Cu(TPyP)Cu ₂ (O ₂ CCH ₃) ₄]/TCNQ	Liquid-liquid interface	TCNQ	10^{-6}	-	[108]
TCNQ@Cu ₃ (BTC) ₂	Liquid phase epitaxy	TCNQ	7×10^{-2}	Electronic devices	[109]
TCNQ-Cu ₃ (BTC) ₂	Liquid phase epitaxy	TCNQ	10^{-3}	Conductometric Immunosensing	[110]

Cu ₃ (BTC) ₂ /TCNQ	Liquid phase epitaxy	TCNQ	10 ⁻¹	Electronic devices	[111]
CO ₃ (NDC) ₃ /I ₂	Layer-by-layer	I ₂	1.88×10 ⁻⁶	Semiconductor	[112]
Cu ₃ BTC ₂ /I ₂	Liquid phase epitaxy	I ₂	2.43×10 ⁻⁶	Solar cells	[113]
Cu-TCNQ-I ₂	Liquid phase epitaxy	I ₂	-	Flexible electronic devices	[114]
Zr-MOF/PAn	Solvotherm (<i>In situ</i>)	PAn	2.10×10 ⁻²	Thermoelectrics	[117]
PPy@UiO-66@CT	Solvotherm (<i>In situ</i>)	PPy	14.29	Supercapacitors	[118]
BMOF/MV ²⁺	Solvotherm (<i>In situ</i>)	MV ²⁺	2.3×10 ⁻⁵	-	[119]
Cu ₃ (HHTP) ₂	Liquid phase epitaxy	Intrinsic	0.02	Chemical resistance sensors	[43]
Ni ₃ HHTP ₂ Ni ₃ HITP ₂	self-assembly	Intrinsic	0.01-2.0	Chemical resistance sensors	[44]
Cu-TCPP-on -Cu-HHTP	Van-der-Waals integration	Intrinsic	-	Chemical resistance sensors	[125]
Cu-HHTP-10C /HITP	Liquid phase epitaxy	HITP	-	Chemical resistance sensors	[126]
Cu-TCPP/PPy	Surfactant-assisted synthesis	PPy	-	Supercapacitors	[45]
Ni-HAB Cu-HAB	Liquid-liquid interfacial	Intrinsic	(70 ± 15)×10 ⁻² (11 ± 3) ×10 ⁻²	Supercapacitors	[129]
Ni ₃ HITP ₂	Gas-liquid interfacial	Intrinsic	-	Supercapacitors	[46]
[Co ₃ (HHTP) ₂] _n	Layer-by-layer	Intrinsic	-	Electrocatalysis (OER)	[131]
NiPc-MOF	bottom-up	Intrinsic	~0.2	Electrocatalysis (OER)	[132]
Ni ₃ (HITP) ₂	Solvotherm (<i>In situ</i>)	Intrinsic	-	Electrocatalysis (ORR)	[135]
Cu ₃ (BTC) ₂	Liquid phase epitaxy	Intrinsic	-	Field effect transistor	[142]
Ni ₃ (HITP) ₂	Gas-liquid interfacial	Intrinsic	40	Field effect transistor	[30]

Ni ₃ (HITP) ₂	Solvotherm (<i>In situ</i>)	Intrinsic	-	Field effect transistor	[29]
Cu ₃ (HHTP) ₂	Liquid phase epitaxy	Intrinsic	0.29	Organic spin valves	[28]

5. Conclusions and Outlook

Recently, conductive MOF films have brought about increasing attention from researchers as a new electronic material due to their diverse structures, adjustable pore structures, and great electrical conductivities. This review systematically summarized the methods for preparing MOF films, for introducing conductivity into MOF films, and the wide range of applications of conductive MOF films in electrochemistry. The methods for synthesizing MOF films include solution-based preparation methods (liquid phase epitaxy, LB-LBL, interface and reverse diffusion synthesis, solvothermal growth from mother solution) and vacuum-based preparation methods (chemical vapor deposition, atomic layer deposition). More importantly, conductive MOF films can be formed by introducing redox active molecules (such as I₂, TCNQ) and conductive polymers (such as PEDOT, PPy) into the MOFs. These conductive films show significant potential in many emerging applications, such as electrochemical sensing, supercapacitors and electrocatalysis (**Table 1**).

Although the study of conductive MOF films has made great progress in recent years, this research area is still in its infancy. Still too many things are not known and therefore further development will have to overcome numerous difficulties and challenges.

First of all, the production of large area conductive MOF films is of great importance for industrial applications, but the currently reported sizes of MOF films are typically few square centimeters. Xu *et al.* prepared a MOF film^[59] with a membrane area of 78 cm² using gas-liquid interfacial synthesis. However, the industrial scale manufacture of the conductive MOF films is still a major challenge.

Secondly, although the conductivity of MOF films is significantly improved by doping conductive molecules into the MOF, the conductivity obtained in current studies is still not very high, and the introduction of conductivity reduces the specific surface area of the MOF film. It is still challenging to enhance the conductivity of the MOF film while maintaining its specific surface area. In addition, there are still too few reports on the introduction of conductive polymers into MOF films.

Finally, conductive MOF films are a promising electronic material that will have rapid and sustained development in electronics and electrochemistry, and will also be applied in other fields, including heterogeneous photocatalysis, optical and optoelectronic devices.

Acknowledgements

W. K. Wang would like to thank Shaanxi University of Science and Technology for start-up funds (2018BJ-67) for young talented researchers. This work was supported by the National Natural Science Foundation of China (NSFC,51903141).

Conflict of Interest

The authors declare no conflict of interest.

Received: ((will be filled in by the editorial staff))

Revised: ((will be filled in by the editorial staff))

Published online: ((will be filled in by the editorial staff))

Reference

- [1] H. C. Zhou, J. R. Long, O. M. Yaghi, *Chem. Rev.* **2012**, *112*, 673.
- [2] S. Kitagawa, R. Kitaura, S. I. Noro, *Angew. Chem. Int. Ed.* **2004**, *43*, 2334.
- [3] B. Li, H. M. Wen, H. L. Wang, H. Wu, T. Yildirim, W. Zhou, B.L. Chen, *Energ & Environ. Sci.* **2015**, *8*, 2504.
- [4] L. J. Murray, M. Dincă, J. R. Long, *Chem. Soc. Rev.* **2009**, *38*, 1294.
- [5] J. R. Li, J. Sculley, H. C. Zhou, *Chem. Rev.* **2012**, *112*, 869.

- [6] T. Rodenas, I. Luz, G. Prieto, B. Seoane, H. Miro, A. Corma, F. Kapteijn, F. X. L. I. Xamena, J. Gascon, *Nat. Mater.* **2015**, *14*, 48.
- [7] L. Jiao, Y. Wang, H. L. Jiang, Q. Xu, *Adv. Mater.* **2017**, *30*, e1703663.
- [8] S. Wang, X. Wang, *Small* **2015**, *11*, 3097.
- [9] J. D. Rocca, D. Liu, W. Lin, *Acc. Chem. Res.* **2011**, *44*, 957.
- [10] L. Sun, M. G. Campbell, M. Dincă, *Angew. Chem. Int. Ed.* **2016**, *55*, 3566.
- [11] S. S. Park, E. R. Hontz, L. Sun, C. H. Hendon, A. Walsh, T. V. Voorhis, M. Dincă, *J. Am. Chem. Soc.* **2015**, *137*, 1774.
- [12] A. J. Clough, N. M. Orchanian, J. M. Skelton, A. J. Neer, S. A. Howard, C. A. Downes, L. F. J. Piper, A. Walsh, B. C. Melot, S. C. Marinescu, *J. Am. Chem. Soc.* **2019**, *141*, 16323.
- [13] D. Y. Lee, E. K. Kim, N. K. Shrestha, D. W. Boukhvalov, J. K. Lee, S. H. Han, *ACS Appl. Mater. Interfaces.* **2015**, *7*, 18501.
- [14] R. Hoffmann, *Acc. Chem. Res.* **1971**, *4*, 1.
- [15] M. Ko, L. Mendecki, K. A. Mirica, *Chem. Commun.* **2018**, *54*, 7873.
- [16] M. G. Campbell, D. Sheberla, S. F. Liu, T. M. Swager, M. Dincă, *Angew. Chem. Int. Ed.* **2015**, *54*, 4349.
- [17] D. Sheberla, J. C. Bachman, J. S. Elias, C. J. Sun, Y. S. Horn, M. Dincă, *Nat. Mater.* **2017**, *16*, 220.
- [18] V. R. Giménez, N. A. Barrios, G. E. Ariza, M. Galbiati, M. Sessolo, S. Tatay, C. M. Gastaldo, *Angew. Chem. Int. Ed.* **2018**, *130*, 15306.
- [19] M. G. Campbell, S. F. Liu, T. M. Swager, M. Dincă, *J. Am. Chem. Soc.* **2015**, *137*, 13780.
- [20] M. K. Smith, K. E. Jensen, P. A. Pivak, K. A. Mirica, *Chem. Mater.* **2016**, *28*, 5264.
- [21] Q. Cheng, K. Tao, X. Han, Y. Yang, Z. Yang, Q. Ma, L. Han, *Dalton. Trans.* **2019**, *48*, 4119.

- [22] L. Wang, X. Feng, L. Ren, Q. Piao, J. Zhong, Y. Wang, Ha. Li, Y. Chen, B. Wang, *J. Am. Chem. Soc.* **2015**, 137, 4920.
- [23] S. Guo, X. Xu, J. Liu, Q. Zhang, H. Wang, *J. Electrochem. Soc.* **2020**, 167, 020539.
- [24] Z. Li, M. Tan, Y. Zheng, Y. Luo, Q. Jing, J. Jiang, M. Li, *J. Inorg. Mater.* **2020**, 35, 769.
- [25] X. Huang, H. Yao, Y. Cui, W. Hao, J. Zhu, W. Xu, D. Zhu, *ACS Appl. Mater. Interfaces.* **2017**, 9, 40752.
- [26] P. M. Usov, B. Huffman, C. C. Epley, M. C. Kessinger, J. Zhu, W. A. Maza, A. J. Morris, *ACS Appl. Mater. Interfaces.* **2017**, 9, 33539.
- [27] A. P. Mártire, G. M. Segovia, O. Azzaroni, M. Rafti, W. Marmisollé, *Mol. Syst. Des. Eng.* **2019**, 4, 893.
- [28] X. Song, X. Wang, Y. Li, C. Zheng, B. Zhang, C. Di, F. Li, C. Jin, W. Mi, L. Chen, W. Hu, *Angew. Chem. Int. Ed.* **2020**, 59, 1911543.
- [29] B. Wang, Y. Luo, B. Liu, G. Duan, *ACS Appl. Mater. Interfaces.* **2019**, 11, 35935.
- [30] G. Wu, J. Huang, Y. Zang, J. He, G. Xu, *J. Am. Chem. Soc.* **2017**, 139, 1360.
- [31] D. Zacher, O. Shekhah, C. Wöll, R. A. Fischer, *Chem. Soc. Rev.* **2009**, 38, 1418.
- [32] H. Zhu, D. Liu, *J. Mater. Chem. A* **2019**, 7, 21004.
- [33] W. Li, *Prog. Mater. Sci.* **2019**, 100, 21.
- [34] O. Shekhah, J. Liu, R. A. Fischer, Ch. Wöll, *Chem. Soc. Rev.* **2011**, 40, 1081.
- [35] J. Meng, X. Liu, C. Niu, Q. Pang, J. Li, F. Liu, Z. Liu, L. Mai, *Chem. Soc. Rev.* **2020**, 49, 3142.
- [36] S. K. Bhardwaj, N. Bhardwaj, R. Kaur, J. Mehta, A. L. Sharma, K. H. Kim, A. Deep, *J. Mater. Chem. A* **2018**, 6, 14992.
- [37] X. Deng, J. Y. Hu, J. Luo, W. M. Liao, J. He, *Top. Curr. Chem.* **2020**, 378, 1.
- [38] W. H. Li, W. H. Deng, G. E. Wang, G. Xu, *EnergyChem* **2020**, 2, 1.
- [39] L. S. Xie, G. Skorupskii, M. Dincă, *Chem. Rev.* **2020**, 120, 8536.
- [40] C. W. Kung, P. C. Han, C. H. Chuang, K. C.-W. Wu, *APL Mater.* **2019**, 7, 110902.

- [41] L. Guo, J. Sun, J. Wei, Y. Liu, L. Hou, C. Yuan, *Carbon Energy* **2020**, 2, 203.
- [42] C. Li, X. Sun, Y. Yao, G. Hong, *Mater. Today. Nano.* **2020**, 13, 100105.
- [43] M. S. Yao, X. J. Lv, Z. H. Fu, W. H. Li, W. H. Deng, G. D. Wu, G. Xu, *Angew. Chem. Int. Ed.* **2017**, 56, 16510.
- [44] M. K. Smith, K. A. Mirica, *J. Am. Chem. Soc.* **2017**, 139, 16759.
- [45] W. Zhao, W. Wang, J. Peng, T. Chen, B. Jin, S. Liu, W. Huang, Q. Zhao, *Dalton. Trans.* **2019**, 48, 9631.
- [46] W. Zhao, T. Chen, W. Wang, B. Jin, J. Peng, S. Bi, M. Jiang, S. Liu, Q. Zhao, W. Huang, *Sci. Bull.* **2020**, 65, 1803.
- [47] G. Jia, W. Zhang, G. Fan, Z. Li, D. Fu, W. Hao, C. Yuan, Z. Zou, *Angew. Chem. Int. Ed.* **2017**, 56, 13781.
- [48] A. P. Mártire, G. M. Segovia, O. Azzaroni, M. Rafti, W. Marmisollé, *Mol. Syst. Des. Eng.* **2019**, 4, 893.
- [49] O. Shekhah, H. Wang, D. Zacher, R. A. Fischer, C. Wöll, *Angew. Chem. Int. Ed.* **2009**, 48, 5038.
- [50] O. Shekhah, H. Wang, S. Kowarik, F. Schreiber, M. Paulus, M. Tolan, C. Sternemann, F. Evers, D. Zacher, R. A. Fischer, C. Wöll, *J. Am. Chem. Soc.* **2007**, 129, 15118.
- [51] S. Sakaida, K. Otsubo, O. Sakata, C. Song, A. Fujiwara, Masaki Takata, H. Kitagawa, *Nat. Mater.* **2016**, 8, 377.
- [52] O. Shekhah, H. Wang, M. Paradinas, C. Ocal, B. Schüpbach, A. Terfort, D. Zacher, R. A. Fischer, C. Wöll, *Nat. Mater.* **2009**, 8, 481.
- [53] M. Zhou, J. Li, M. Zhang, H. Wang, Y. Lan, Y. N. Wu, F. Li, G. Li, *Chem. Commun.* **2015**, 51, 2706.
- [54] J. Zhao, B. Gong, W. T. Nunn, P. C. Lemaire, E. C. Stevens, F. I. Sidi, P. S. Williams, C. J. Oldham, H. J. Walls, S. D. Shepherd, M. A. Browe, G. W. Peterson, M. D. Losegod, G. N. Parsons, *J. Mater. Chem. A* **2015**, 3, 1458.

- [55] V. Chernikova, O. Shekhah, M. Eddaoudi, *ACS Appl. Mater. Interfaces*. **2016**, *8*, 20459.
- [56] R. Dong, M. Pfeffermann, H. Liang, Z. Zheng, X. Zhu, J. Zhang, X. Feng, *Angew. Chem. Int. Ed.* **2015**, *54*, 12058.
- [57] R. Dong, Z. Zheng, D. C. Tranca, J. Zhang, N. Chandrasekhar, S. Liu, X. Zhuang, G. Seifert, X. Feng, *Chem. Eur. J.* **2017**, *23*, 2255.
- [58] R. Makiura, S. Motoyama, Y. Umemura, H. Yamanaka, O. Sakata, H. Kitagawa, *Nat. Mater.* **2010**, *9*, 565.
- [59] S. Motoyama, R. Makiura, O. Sakata, H. Kitagawa, *J. Am. Chem. Soc.* **2011**, *133*, 5640.
- [60] R. Ameloot, F. Vermoortele, W. Vanhove, M. B. J. Roeffaers, B. F. Sels, D. E. De Vos, *Nat. Chem.* **2011**, *3*, 382.
- [61] T. Kambe, R. Sakamoto, K. Hoshiko, K. Takada, M. Miyachi, J. Heun Ryu, S. Sasaki, J. Kim, K. Nakazato, M. Takata, H. Nishihara, *J. Am. Chem. Soc.* **2013**, *135*, 2462.
- [62] X. Huang, P. Sheng, Z. Tu, F. Zhang, J. Wang, H. Geng, Y. Zou, C. A. Di, Y. Yi, Y. Sun, W. Xu, D. Zhu, *Nat. Commun.* **2015**, *6*, 7408.
- [63] J. Liu, C. Wöll, *Chem. Soc. Rev.* **2017**, *46*, 5730.
- [64] X. J. Bai, D. Chen, L. L. Li, L. Shao, W. X. He, H. Chen, Y. N. Li, X. M. Zhang, L. Y. Zhang, T. Q. Wang, Y. Fu, W. Qi, *ACS Appl. Mater. Interfaces*. **2018**, *10*, 25960.
- [65] R. Makiura, O. Kononov, *Sci. Rep.* **2013**, *3*, 2506.
- [66] Y. Zang, F. Pei, J. Huang, Z. Fu, G. Xu, X. Fang, *Adv. Energy Mater.* **2018**, *31*, 1802052.
- [67] J. Yao, D. Dong, D. Li, L. He, G. Xu, H. Wang, *Chem. Commun.* **2011**, *47*, 2559.
- [68] K. Huang, Q. Li, G. Liu, J. Shen, K. Guan, W. Jin, *ACS Appl. Mater. Interfaces*. **2015**, *7*, 16157.
- [69] H. T. Kwon, H. K. Jeong, *J. Am. Chem. Soc.* **2013**, *135*, 10763.
- [70] D. Bradshaw, A. Garai, J. Huo, *Chem. Soc. Rev.* **2012**, *41*, 2344.
- [71] C. W. Kung, T. H. Chang, L. Y. Chou, J. T. Hupp, O. K. Farha, K. C. Ho, *Chem. Commun.* **2015**, *51*, 2414.

- [72]M. Shah, H. T. Kwon, V. Tran, S. Sachdeva, H. K. Jeong, *Microporous. Mesoporous. Mater.* **2013**, *165*, 63.
- [73]W. J. Li, S. Y. Gao, T. F. Liu, L. W. Han, Z. J. Lin, R. Cao, *Langmuir*. **2013**, *29*, 8657.
- [74]D. Jiang, A. D. Burrows, R. Jaber, K. J. Edler, *Chem. Commun.* **2012**, *48*, 4965.
- [75]M. Miyamoto, S. Kohmura, H. Iwatsuka, Y. Oumic, S. Uemiya, *CrystEngComm*. **2015**, *17*, 3422.
- [76]D. B. Dwyer, D. T. Lee, S. Boyer, W. E. Bernier, G. N. Parsons, W. E. Jones, Jr, *ACS Appl. Mater. Interfaces*. **2018**, *10*, 30.
- [77]A. Betard, R. A. Fischer, *Chem. Rev.* **2012**, *112*, 1055.
- [78]R. Ranjan, M. Tsapatsis, *Chem. Mater.* **2009**, *21*, 4920.
- [79]J. Nan, X. Dong, W. Wang, W. Jin, N. Xu, *Langmuir* **2011**, *27*, 4309.
- [80]J. Zhang, T. Xia, D. Zhao, Y. Cui, Y. Yang, G. Qian, *Sens. Actuators B Chem.* **2018**, *260*, 63.
- [81]W. J. Li, M. Tu, R. Cao, R. A. Fischer, *J. Mater. Chem. A* **2016**, *4*, 12356.
- [82]U. Müller, H. Pütter, M. Hesse, H. Wessel, M. Schubert, J. Huff, M. Guymann, WO Patent, WO/2005/049892, **2005**.
- [83]Z. Zhuang., D. Liu, *Nano-Micro. Lett.* DOI:10.1007/s40820-020-00470-w.
- [84]S. Alizadeh, D. Nematollahi, *J. Am. Chem. Soc.* **2017**, *139*, 4753.
- [85]J. L. Hauser, M. Tso, K. Fitchmun, S. R. J. Oliver, *Cryst. Growth Des.* **2019**, *19*, 2358.
- [86]R. Ameloot, L. Stappers, J. Fransaer, L. Alaerts, B. F. Sels, D. E. De Vos, *Chem. Mater.* **2009**, *21*, 2580.
- [87]N. Campagnol, T. V. Assche, T. Boudewijns, J. Denayer, K. Binnemans, D. D. Vos, J. Fransaer, *J. Mater. Chem. A* **2013**, *1*, 5827.
- [88]W. J. Li, J. Lü, S. Y. Gao, Q. H. Li, R. Cao, *J. Mater. Chem. A* **2014**, *2*, 19473.
- [89]W. J. Li, J. Liu, Z. H. Sun, T. F. Liu, J. Lü, S. Y. Gao, C. He, R. Cao, J. H. Luo, *Nat. Commun.* **2016**, *7*, 11830.

- [90] I. Hod, W. Bury, D. M. Karlin, P. Deria, C. W. Kung, M. J. Katz, M. So, B. Klahr, D. Jin, Y. W. Chung, T. W. Odom, O. K. Farha, J. T. Hupp, *Adv. Mater.* **2014**, *26*, 6295.
- [91] H. Zhu, H. Liu, I. Zhitomirsky, S. Zhu, *Mater. Lett.* **2015**, *142*, 19.
- [92] M. Li, M. Dincă, *J. Am. Chem. Soc.* **2011**, *133*, 12926.
- [93] M. Li, M. Dincă, *Chem. Sci.* **2014**, *5*, 107.
- [94] I. Stassen, D. D. Vos, R. Ameloot, *Chem. Eur. J.* **2016**, *22*, 14452.
- [95] I. Stassen, M. Styles, G. Greci, H. V. Gorp, W. Vanderlinden, S. D. Feyter, P. Falcaro, D. D. Vos, P. Vereecken, R. Ameloot, *Nat. Mater.* **2016**, *15*, 304.
- [96] T. Stassin, I. Stassen, J. Marreiros, A. J. Cruz, R. Verbeke, M. Tu, H. Reinsch, M. Dickmann, W. Egger, I. F. J. Vankelecom, D. D. Vos, R. Ameloot, *Chem. Mater.* **2020**, *32*, 1784.
- [97] T. Stassin, S. R. Hermida, B. Schrode, A. J. Cruz, F. Carraro, D. Kravchenko, V. Creemers, I. Stassen, T. Hauffman, D. D. Vos, P. Falcaro, R. Resel, R. Ameloot, *Chem. Commun.* **2019**, *55*, 10056.
- [98] J. K. Huang, N. Saito, Y. Cai, Y. Wan, C. C. Cheng, M. Li, J. Shi, K. Tamada, V. C. Tung, S. Li, L. J. Li, *ACS. Materials. Lett.* **2020**, *2*, 485.
- [99] S. M. George, *Chem. Rev.* **2010**, *110*, 111.
- [100] E. Ahvenniemi, M. Karppinen, *Chem. Commun.* **2016**, *52*, 1139.
- [101] L. D. Salmi, M. J. Heikkilä, E. Puukilainen, T. Sajavaara, D. Grosso, M. Ritala, *Microporous. Mesoporous. Mater.* **2013**, *182*, 147.
- [102] E. Ahvenniemi, M. Karppinen, *Chem. Mater.* **2016**, *28*, 6260.
- [103] X. Sun, K. H. Wu, R. Sakamoto, T. Kusamoto, H. Maeda, X. Ni, W. Jiang, F. Liu, S. Sasaki, H. Masunaga, H. Nishihara, *Chem. Sci.* **2017**, *8*, 8078.
- [104] D. Sheberla, L. Sun, M. A. Blood-Forsythe, S. Er, C. R. Wade, C. K. Brozek, A. Aspuru-Guzik, M. Dincă, *J. Am. Chem. Soc.* **2014**, *136*, 8859.
- [105] I. F. Chen, C. F. Lu, W. F. Su, *Langmuir.* **2018**, *34*, 15754.

- [106] L. Sun, C. H. Hendon, M. A. Minier, A. Walsh, M. Dincă, *J. Am. Chem. Soc.* **2015**, *137*, 6164.
- [107] S. L. Cai, Y. B. Zhang, A. B. Pun, B. He, J. Yang, F. M. Toma, I. D. Sharp, O. M. Yaghi, J. Fan, S. R. Zheng, W. G. Zhang, Y. Liu, *Chem. Sci.* **2014**, *5*, 4693.
- [108] A. Sengupta, S. Datta, C. Su, T. S. Heng, J. Ding, J. J. Vittal, K. P. Loh, *ACS Appl. Mater. Interfaces.* **2016**, *8*, 16154.
- [109] A. A. Talin, A. Centrone, A. C. Ford, M. E. Foster, V. Stavila, P. Haney, R. A. Kinney, V. Szalai, F. E. Gabaly, H. P. Yoon, F. Léonard, M. D. Allendorf, *Science* **2014**, *343*, 66.
- [110] S. K. Bhardwaj, A. L. Sharma, N. Bhardwaj, M. Kukkar, A. A. S. Gill, K. H. Kim, A. Deep, *Sens. Actuators B Chem.* **2017**, *240*, 10.
- [111] K. Thürmer, C. Schneider, V. Stavila, R. W. Friddle, F. Léonard, R. A. Fischer, M. D. Allendorf, A. A. Talin, *ACS Appl. Mater. Interfaces.* **2018**, *10*, 39400.
- [112] D. Y. Lee, E. K. Kim, N. K. Shrestha, D. W. Boukhvalov, J. K. Lee, S. H. Han, *ACS Appl. Mater. Interfaces.* **2015**, *7*, 18501.
- [113] D. Y. Lee, D. V. Shinde, S. J. Yoon, K. N. Cho, W. Lee, N. K. Shrestha, S. H. Han, *J. Phys. Chem. C* **2014**, *118*, 16328.
- [114] S. Rana, R. Rajendra, B. Dhara, P. K. Jha, N. Ballav, *Adv. Mater. Interfaces.* **2016**, *3*, 1500738.
- [115] B. L. Ouay, T. Uemura, *Isr. J. Chem.* **2018**, *58*, 1.
- [116] T. Kitao, Y. Zhang, S. Kitagawa, B. Wang, T. Uemura, *Chem. Soc. Rev.* **2017**, *46*, 3108.
- [117] C. C. Lin, Y. C. Huang, M. Usman, W. H. Chao, W. K. Lin, T. T. Luo, W. T. Whang, C. H. Chen, K. L. Lu, *ACS Appl. Mater. Interfaces.* **2019**, *11*, 3400.
- [118] C. Zhang, J. Tian, W. Rao, B. Guo, L. Fan, W. Xu, J. Xu, *Cellulose* **2019**, *26*, 3387.

- [119] Z. Guo, D. K. Panda, K. Maity, D. Lindsey, T. G. Parker, T. E. Albrecht-Schmitt, J. L. Barreda-Esparza, P. Xiong, W. Zhou, S. Saha, *J. Mater. Chem. C* **2016**, *4*, 894.
- [120] R. S. Lokey, B. L. Iverson, *Nature* **1995**, *375*, 303.
- [121] C. R. Martinez, B. L. Iverson, *Chem. Sci.* **2012**, *3*, 2191.
- [122] D. D. Lee, D. S. Lee, *IEEE. Sens. J.* **2001**, *1*, 214.
- [123] G. Konvalina, H. Haick, *Acc. Chem. Res.* **2014**, *47*, 66.
- [124] S. Su, W. Wu, J. Gao, J. Lu, C. Fan, *J. Mater. Chem.* **2012**, *22*, 18101.
- [125] M. S. Yao, J. W. Xiu, Q. Q. Huang, W. H. Li, W. W. Wu, A. Q. Wu, L. A. Cao, W. H. Deng, G. E. Wang, G. Xu, *Angew. Chem. Int. Ed.* **2019**, *58*, 14915.
- [126] A. Q. Wu, W. Q. Wang, H. B. Zhan, L. A. Cao, X. L. Ye, J. J. Zheng, P. N. Kumar, K. Chiranjeevulu, W. H. Deng, G. E. Wang, M. S. Yao, G. Xu, *Nano Res.* DOI: 10.1007/s12274-020-2823-8.
- [127] P. Simon, Y. Gogotsi, *Nanosci. Technol.* **2009**, *7*, 320.
- [128] X. Chen, R. Paul, L. Dai, *Natl. Sci. Rev.* **2017**, *4*, 453.
- [129] D. Feng, T. Lei, M. R. Lukatskaya, J. Park, Z. Huang, M. Lee, L. Shaw, S. Chen, A. A. Yakovenko, A. Kulkarni, J. Xiao, K. Fredrickson, J. B. Tok, X. Zou, Y. Cui, Z. Bao, *Nat. Energy* **2018**, *3*, 30.
- [130] I. Hod, P. Deria, W. Bury, J. E. Mondloch, C. W. Kung, M. So, M. D. Sampson, A. W. Peters, C. P. Kubiak, O. K. Farha, J. T. Hupp, *Nat. Commun.* **2015**, *6*, 8304.
- [131] M. Zhang, B. H. Zheng, J. Xu, N. Pan, J. Yu, M. Chen, H. Cao, *Chem. Commun.* **2018**, *54*, 13579.
- [132] H. Jia, Y. Yao, J. Zhao, Y. Gao, Z. Luo, P. Du, *J. Mater. Chem. A* **2018**, *6*, 1188.
- [133] M. K. Gulbinska, *Lithium-ion Battery Materials and Engineering*, Springer-Verlag. London **2014**.
- [134] V. R. Stamenkovic, B. Fowler, B. S. Mun, G. Wang, P. N. Ross, C. A. Lucas, N. M. Marković, *Science* **2007**, *315*, 493.

- [135] E. M. Miner, T. Fukushima¹, D. Sheberla, L. Sun, Y. Surendranath, M. Dincă, *Nat. Commun.* **2016**, *7*, 10942.
- [136] G. C. Dacey, I. M. Ross, *Bell Syst. Tech. J.* **1955**, *34*, 1149.
- [137] Z. Meng, A. Aykanat, K. A. Mirica, *J. Am. Chem. Soc.* **2019**, *141*, 2046.
- [138] M. N. M. N, U. Hashim, M. K. M. Arshad, S. R. Kasjoo, S. F. A. Rahman, A. R. Ruslinda, M. F. M. Fathil, R. Adzhri, M. M. Shahimin, *Biosens. Bioelectron.* **2016**, *83*, 106.
- [139] K. Zagorodniy, G. Seifert, H. Hermann, *Appl. Phys. Lett.* **2010**, *97*, 251905.
- [140] E. Redel, Z. Wang, S. Walheim, J. Liu, H. Gliemann, C. Wöll, *Appl. Phys. Lett.* **2013**, *103*, 091903.
- [141] Z. G. Gu, L. Heinke, C. Wöll, T. Neumann, W. Wenzel, Q. Li, K. Fink, O. D. Gordan, D. R. T. Zahn, *Appl. Phys. Lett.* **2015**, *107*, 183301.
- [142] Z. G. Gu, S. C. Chen, W. Q. Fu, Q. Zheng, J. Zhang, *ACS Appl. Mater. Interfaces.* **2017**, *9*, 7259.
- [143] S. A. Wolf, D. D. Awschalom, R. A. Buhrman, J. M. Daughton, S. von Molnár, M. L. Roukes, A. Y. Chtchelkanova, D. M. Treger, *Science* **2001**, *294*, 1488.
- [144] V. A. Dediu, L. E. Hueso, I. Bergenti, C. Taliani, *Nat. Mater.* **2009**, *8*, 707.

Recently, conductive MOF films have brought about increasing attention from researchers as a new electronic material due to their diverse structures, adjustable pore structures, and great electrical conductivities. This review systematically summarizes the methods for preparing MOF films, for introducing conductivity into MOF films, and the wide range of applications of conductive MOF films in electrochemistry. Finally, the current challenges for conductive MOF films are also highlighted.

X. Y. Mu, W. K. Wang,* C. C. Sun, J. L. Wang, C. B. Wang,* and M. Knez*

Recent Progress on Conductive Metal-Organic Framework Films

ToC figure

